A REVIEW OF CLIMATIC CONTROLS ON $\delta^{18}O$ IN PRECIPITATION OVER THE TIBETAN PLATEAU: OBSERVATIONS AND SIMULATIONS

Tandong Yao,[1,2] Valerie Masson-Delmotte,[3] Jing Gao,[1] Wusheng Yu,[1] Xiaoxin Yang,[1] Camille Risi,[4] Christophe Sturm,[5] Martin Werner,[6] Huabiao Zhao,[1] You He,[1] Wei Ren,[1] Lide Tian,[1,2] Chunming Shi,[3] and Shugui Hou[2,7]

Received 26 November 2012; revised 20 September 2013; accepted 22 September 2013; published 1 November 2013.

[1] The stable oxygen isotope ratio ($\delta^{18}O$) in precipitation is an integrated tracer of atmospheric processes worldwide. Since the 1990s, an intensive effort has been dedicated to studying precipitation isotopic composition at more than 20 stations in the Tibetan Plateau (TP) located at the convergence of air masses between the westerlies and Indian monsoon. In this paper, we establish a database of precipitation $\delta^{18}O$ and use different models to evaluate the climatic controls of precipitation $\delta^{18}O$ over the TP. The spatial and temporal patterns of precipitation $\delta^{18}O$ and their relationships with temperature and precipitation reveal three distinct domains, respectively associated with the influence of the westerlies (northern TP), Indian monsoon (southern TP), and transition in between. Precipitation $\delta^{18}O$ in the monsoon domain experiences an abrupt decrease in May and most depletion in August, attributable to the shifting moisture origin between Bay of Bengal (BOB) and southern Indian Ocean. High- resolution atmospheric models capture the spatial and temporal patterns of precipitation $\delta^{18}O$ and their relationships with moisture transport from the westerlies and Indian monsoon. Only in the westerlies domain are atmospheric models able to represent the relationships between climate and precipitation $\delta^{18}O$. More significant temperature effect exists when either the westerlies or Indian monsoon is the sole dominant atmospheric process. The observed and simulated altitude-$\delta^{18}O$ relationships strongly depend on the season and the domain (Indian monsoon or westerlies). Our results have crucial implications for the interpretation of paleoclimate records and for the application of atmospheric simulations to quantifying paleoclimate and paleo-elevation changes.

Citation: Yao, T., et al. (2013), A review of climatic controls on $\delta^{18}O$ in precipitation over the Tibetan Plateau: Observations and simulations, *Rev. Geophys.*, *51*, 525–548, doi:10.1002/rog.20023.

1. INTRODUCTION

[2] With an average altitude above 4000 m, a vast geographical coverage, and large-scale climatic influence, the Tibetan Plateau (TP) is considered as the "Third Pole" of the Earth. The elevated topography of the TP does not only act as a barrier to the midlatitude westerlies but also strengthens the Indian monsoon through its dynamical and thermal impacts, thus contributing to large-scale atmospheric circulation [*Bothe et al.*, 2011]. In turn, the influences of the westerlies and Indian monsoon (Figure 1a) are critical for advection of heat and moisture, and climate patterns in the TP region [*An et al.*, 2001, 2012]. The TP snow cover and albedo are known to have large-scale impacts on atmospheric circulation [*Wu and Qian*, 2003; *Ma et al.*, 2009; *Kang et al.*, 2010; *Poulsen and Jeffery*, 2011]. The TP is particularly sensitive to climate change and regional anthropogenic forcing [*Xu et al.*, 2009] and currently experiencing significant warming [*Yao et al.*, 1996a; *Liu and Chen*, 2000; *Tian et al.*, 2006; *Kang et al.*, 2007; *Qin et al.*, 2009] with important impacts on biodiversity and environment [*Klein et al.*, 2004; *Wang et al.*, 2008]. The TP also acts as a water tower for surrounding regions due to monsoon precipitation and glacier melt [*Barnett et al.*, 2005; *Yao et al.*, 2007; *Viviroli et al.*, 2007; *Bates et al.*,

[1]Key Laboratory of Tibetan Environment Changes and Land Surface Processes, Institute of Tibetan Plateau Research, Chinese Academy of Sciences, Beijing, China.
[2]State Key Laboratory of Cryospheric Sciences, Cold and Arid Regions Environmental and Engineering Research Institute, Chinese Academy of Sciences, Lanzhou, China.
[3]LSCE, UMR 8212, IPSL, CEA/CNRS/UVSQ, Gif-sur-Yvette, France.
[4]LMD, IPSL, CNRS/UPMC, Paris, France.
[5]Bert Bolin Centre for Climate Research and Department of Geological Sciences, Stockholm University, Stockholm, Sweden.
[6]Alfred Wegener Institute for Polar and Marine Research, Bremerhaven, Germany.
[7]Key Laboratory for Coast and Island Development of Ministry of Education, School of Geographic and Oceanographic Sciences, Nanjing University, Nanjing, China.

Corresponding authors: T. Yao and J. Gao, Key Laboratory of Tibetan Environment Changes and Land Surface Processes, Institute of Tibetan Plateau Research, Chinese Academy of Sciences, Beijing 100101, China. (tdyao@itpcas.ac.cn; gaojing@itpcas.ac.cn)

8755-1209/13/10.1002/rog.20023
2012RG000427

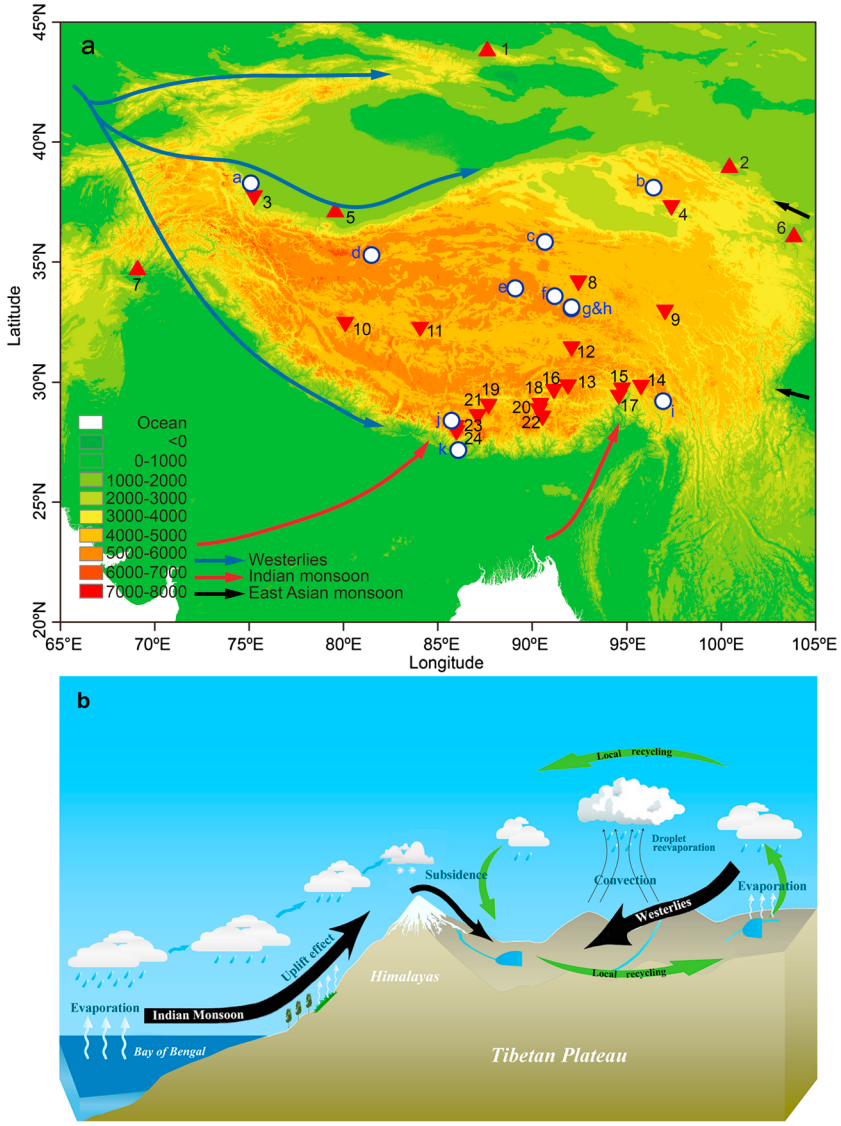

Figure 1. (a) General patterns of moisture transport under the influences of the westerlies and Indian monsoon over the TP. Red triangles depict locations of $\delta^{18}O$ monitoring stations: 1-Urumqi, 2-Zhangye, 3-Taxkorgen, 4-Delingha, 5-Hetian, 6-Lanzhou, 7-Kabul, 8-Tuotuohe, 9-Yushu, 10-Shiquanhe, 11-Gaize, 12-Nagqu, 13-Yangcun, 14-Bomi, 15-Lulang, 16-Lhasa, 17-Nuxia, 18-Baidi, 19-Larzi, 20-Wengguo, 21-Dingri, 22-Dui, 23-Nyalam, 24-Zhangmu; open circles show ice core sites: a-Muztagata, b-Dunde, c-Malan, d-Guliya, e-Puruogangri, f-Geladandong, g-Tanggula 1, h-Tanggula 2, i-Zuoqiupu, j-Dasuopu, k-East Rongbuk. Up triangles stand for GNIP stations and down triangles stand for TNIP stations. (b) Schematic representation of the main processes affecting precipitation $\delta^{18}O$ over the TP.

2008; *Immerzeel et al.*, 2010; *Bolch et al.*, 2012; *Gardelle et al.*, 2012; *Jacob et al.*, 2012]. These features motivate the need for an observation modeling-based understanding of the large-scale (moisture transport) and local-scale (evaporation) atmospheric processes controlling the TP water cycle.

[3] Water stable isotopes ($H_2{}^{18}O$, $H_2{}^{17}O$, HDO, usually expressed in a delta notation as $\delta^{18}O$, $\delta^{17}O$, δD, but restricted to $\delta^{18}O$ in this study) are integrated tracers of the atmospheric processes [*Dansgaard*, 1964; *Craig and Gordon*, 1965] with applications for atmospheric dynamics [*Vimeux et al.*, 2005, 2011; *Tian et al.*, 2007; *Risi et al.*, 2008a, 2010a; *Gao et al.*, 2011], hydrology [*Gao et al.*, 2009; *Landais et al.*, 2010], cloud processes [*Schmidt et al.*, 2005; *Risi et al.*, 2012a, 2012b], and quantitative estimations of past regional climate change from natural archives of past precipitation isotopic composition [*Thompson*, 2000; *Ramirez et al.*, 2003; *Yao et al.*, 2008; *Liang et al.*, 2009; *Cai et al.*, 2010].

[4] Over the TP, precipitation $\delta^{18}O$ reflects integrated information of the interaction between the westerlies and Indian monsoon, combined with local recycling which is characterized by evaporation, convection, and droplet reevaporation (Figure 1b). Therefore, the TP offers both an exceptional access to multiple processes affecting present-day and past precipitation isotopic composition and an exceptional complexity for modeling and data interpretation.

[5] Since the 1960s, the documentation of precipitation isotopic composition has emerged, thanks to monitoring stations ran at monthly or event bases. In parallel, water stable

TABLE 1. Summary Data for 24 Precipitation-Sampling Stations From the TNIP and the GNIP[a]

No.	Station	Latitude	Longitude	Altitude (m)	*n*	Annual *P*	Average *T*	JJA Weighted $\delta^{18}O$	DJF Weighted $\delta^{18}O$	Annual Weighted $\delta^{18}O$	Database
1	**Zhangmu**	27°59′N	85°59′E	2239	71	1318	16.3	−13.2			TNIP
2	**Nyalam**	28°11′N	85°58′E	3810	776	590	3.3	−14.7	−10.8	−12.4	TNIP
3	**Dui**	28°35′N	90°32′E	5030	152	290	−0.9	−19.0	−6.8	−18.6	TNIP
4	**Dingri**	28°39′N	87°07′E	4330	285	265	7.1	−18.2	−15.4	−18.1	TNIP
5	**Wengguo**	28°54′N	90°21′E	4500	90	253	4	−17.6		−16.5	TNIP
6	**Larzi**	29°05′N	87°41′E	4000	41	216	13.7	−20.3			TNIP
7	**Baidi**	29°07′N	90°26′E	4430	171	313	1.2	−17.1	−17.2	−15.7	TNIP
8	**Nuxia**	29°28′N	94°34′E	2780	88	347	11.9	−13.8			TNIP
9	**Lhasa**	29°42′N	91°08′E	3658	1041	417	6.3	−17.3	−11.7	−16.2	TNIP
10	**Lulang**	29°46′N	94°44′E	3327	119	467	5.7	−14.7	−19.1	−14.5	TNIP
11	**Bomi**	29°52′N	95°46′E	2737	111	431	8.4	−14.0	−13.3	−11.8	TNIP
12	**Yangcun**	29°53′N	91°53′E	3500	57	296	10.4	−18.2		−15.9	TNIP
13	**Nagqu**	31°29′N	92°04′E	4508	1132	500	−0.3	−17.0	−17.8	−16.5	TNIP
14	**Gaize**	32°18′N	84°04′E	4430	322	229	−1	−10.6	−17.4	−12.3	TNIP
15	**Shiquanhe**	32°30′N	80°05′E	4278	96	82	0.5	−14.3	−18.8	−14.4	TNIP
16	**Yushu**	33°01′N	97°01′E	3682	536	386	3.6	−13.2	−15.7	−13.1	TNIP
17	**Tuotuohe**	34°13′N	92°26′E	4533	1022	204	−1.3	−10.9	−21.6	−11.9	TNIP
18	Kabul	34°40′N	69°05′E	1860	109	330	11.6	0.4	−10.5	−7.2	GNIP
19	Lanzhou	36°03′N	103°51′E	1517	41	322	10.4	−4.6	−13.0	−5.6	GNIP TNIP
20	Hetian	37°05′N	79°34′E	1375	47	209	9.1	−2.2	−17.8	−5.5	GNIP TNIP
21	**Delingha**	37°22′N	97°22′E	2981	833	186	2.2	−6.3	−19.9	−7.7	TNIP
22	Taxkorgen	37°46′N	75°16′E	3100	143	115	1.6	−3.1	−21.0	−6.8	TNIP
23	**Zhangye**	38°56′N	100°26′E	1483	75	154	7.8	−4.3	−18.7	−6.0	GNIP TNIP
24	Urumqi	43°48′N	87°36′E	918	119	304	7.4	−6.3	−20.6	−10.8	GNIP

[a]For each location, the database has undergone systematic quality control considering the following factors: (i) precise $\delta^{18}O$ measurements (analytical uncertainty of 0.2‰ or better), (ii) duration of the sampling period, and (iii) obvious aberrant values ($\delta^{18}O$ data which are larger than 5‰ and strongly deviate from surrounding $\delta^{18}O$ data are removed). Stations with event-based $\delta^{18}O$ observations are highlighted in bold. Data at Yangcun, Nuxia, Larzi, Dingri, and Zhangmu are shorter than 1 year and the annual $\delta^{18}O$ for those stations are amount-weighted $\delta^{T8}O$ averages of available months.

isotope modeling has evolved from simple Rayleigh distillation models [*Dansgaard*, 1964; *Craig and Gordon*, 1965] to the introduction of water $\delta^{18}O$ in complex atmospheric general circulation models [*Joussaume et al*., 1984; *Jouzel et al*., 1987; *Hoffmann et al*., 1998; *Mathieu et al*., 2002; *Noone and Simmonds*, 2002; *Lee et al*., 2007; *Schmidt et al*., 2007; *Yoshimura et al*., 2008; *Tindall et al*., 2009; *Noone and Sturm*, 2010; *Risi et al*., 2010a], and more recently in regional atmospheric models [*Sturm et al*., 2005, 2007a, 2007b; *Yoshimura et al*., 2010; *Pfahl et al*., 2012] and convection models [*Risi et al*., 2008b]. Progress in the process-based understanding of the large-scale and local drivers of precipitation $\delta^{18}O$ arises from the new data and the synergy between data and models for present or past climates.

[6] An important progress in the model-data comparison has been achieved in performing $\delta^{18}O$ simulations at sufficient spatial resolution to capture regional water cycle processes and nudged to atmospheric reanalyses providing realistic synoptic atmospheric patterns [*Yoshimura et al*., 2008]. The comparison of nudged simulation outputs with station $\delta^{18}O$ provides a quantitative and physically based understanding of the processes controlling precipitation $\delta^{18}O$. It also provides a tool that is complementary to the classical meteorological information to evaluate the key processes of the water cycle [*Yoshimura et al*., 2003; *Risi et al*., 2010a].

[7] Systematic monitoring efforts for TP water $\delta^{18}O$ (Table 1) started in the 1980s, later than those for other regions [*Rozanski et al*., 1992; *Araguás-Araguás et al*., 1998]. The monitoring efforts were initiated with ice coring in the 1980s [*Thompson et al*., 1989; *Yao et al*., 1991] and followed by station sampling [*Yao et al*., 1991, 1996a, 1999; *Zhang et al*., 1995; *Tian et al*., 2003; *Yu et al*., 2008; *Yang et al*., 2012]. The station sampling has been developed into a network of more than 30 stations with 19 stations running continuously and systematically (Figure 1a and Table 1). Later on, event-based sampling of precipitation $\delta^{18}O$ has been carried out within the China Network of Isotope in River and Precipitation (CNIRP) and the Tibetan Observation and Research Platform (TORP) at more than 40 stations on the TP and surrounding regions. Within the Global Network of Isotopes in Precipitation (GNIP) ran by the International Atomic Energy Agency (IAEA), monthly precipitation data have been collected since the 1980s at Lhasa. In the following discussion, we refer to precipitation sampling as station $\delta^{18}O$, all these data embedded in precipitation $\delta^{18}O$, and to those from firn and ice core measurements as ice core $\delta^{18}O$.

[8] Pioneering studies have revealed obvious positive relationship between water $\delta^{18}O$ and temperature in the northern TP and Tianshan Mountains [*Yao and Thompson*, 1992; *Yao et al*., 1996a, 1999; *Zhang et al*., 1995; *Tian et al*., 2001b]. Data in the northern TP evidenced a strong seasonal cycle, with maximum values in summer and minimum values in winter, which are similar to results from other nonmonsoon regions. However, the southern TP precipitation $\delta^{18}O$ was

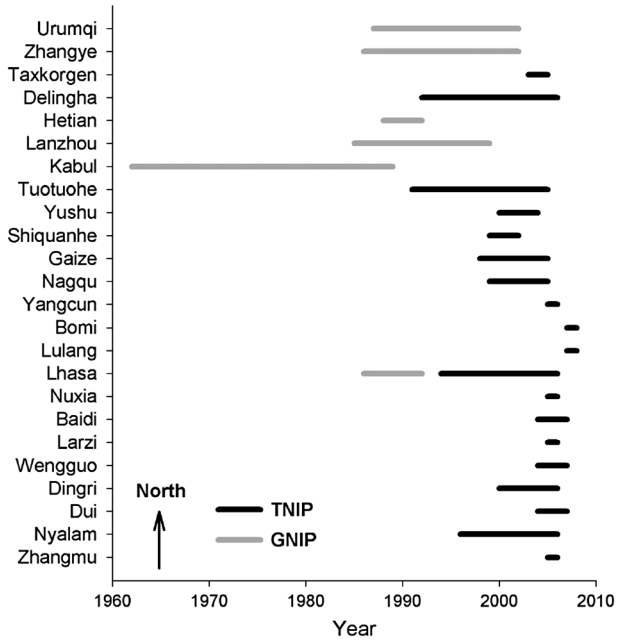

Figure 2. Time span of the database referred to in this paper available for the monthly GNIP stations (grey) and event-based TNIP stations (black). Stations are ordered from south (bottom) to north (top).

revealed to be progressively depleted over the course of the monsoon season, from June to September [*Yao et al*., 1991]. Several studies related the spatial variation of the TP precipitation $\delta^{18}O$ to the complexity of moisture sources and transports [*Aizen et al*., 1996; *Araguás-Araguás et al*., 1998; *Aggarwal et al*., 2004]. Different seasonalities of precipitation $\delta^{18}O$ were used to delimitate the influence of monsoon moisture flow into the TP [*Tian et al*., 2005, 2007; *Yu et al*., 2008, 2009].

[9] Different speculations have been proposed on the mechanisms relating monsoon circulation to the TP precipitation $\delta^{18}O$. The uplift of monsoon moisture flow due to high TP altitude is found to impact $\delta^{18}O$ because of the well-known altitude effect on precipitation $\delta^{18}O$ [*Molnar et al*., 1993; *Liu et al*., 2003]. Recent modeling studies have highlighted the importance of upstream distillation linked with convection and the relationship between water $\delta^{18}O$ and large-scale Asian monsoon circulation at the interannual [*Vuille et al*., 2005], millennial [*Pausata et al*., 2011] and orbital [*LeGrande and Schmidt*, 2009] time scales. Atmospheric general circulation models (GCMs) equipped with water $\delta^{18}O$ can therefore help interpret $\delta^{18}O$ observations and further understand the processes relating to moisture advection and precipitation $\delta^{18}O$ [*Lee et al*., 2011]. Modeling results also demonstrate that the climate effect on precipitation $\delta^{18}O$ does influence paleo-elevation estimation [*Rowley et al*., 2001; *Bershaw et al*., 2012]. Comparing GCMs with $\delta^{18}O$ observations helps to evaluate the deficiencies in the simulated hydrological cycle and to diagnose artifacts in atmospheric model physics [*Schmidt et al*., 2007; *Risi et al*., 2010b].

[10] In this review, we compile a database including station $\delta^{18}O$ and ice core $\delta^{18}O$ in the TP region to address spatial and temporal differences of precipitation $\delta^{18}O$ with consideration of the effect of large-scale atmospheric processes (the westerlies versus Indian monsoon) and local factors, such as geography (latitude and altitude) and local climate parameters (temperature and precipitation amount). We compare the observations with simulations to understand the atmospheric controls on precipitation $\delta^{18}O$ and to assess the ability of models to capture the driving mechanisms of $\delta^{18}O$ variations. Although deuterium measurements allow to test the quality of the sample preservation and to investigate deuterium excess in relationship with water cycle processes [*Tian et al*., 2005; *Hren et al*., 2009], few long deuterium records on high resolution are available for the TP and we decided to focus this paper on precipitation $\delta^{18}O$ data. We do not use measurements of $\delta^{18}O$ in TP river waters either, which are available from sporadic sampling only.

[11] Section 2 describes the databases studied in this paper, and the atmospheric model simulations, while section 3 investigates the relationships between large-scale atmospheric circulation and $\delta^{18}O$ based on observations and three atmospheric models equipped with stable isotopes, including moisture origin diagnostics. The relationships between precipitation $\delta^{18}O$ with temperature and precipitation amount (section 4) are investigated through observations and simulations. Section 5 is dedicated to the spatial and temporal characteristics of the relationship between $\delta^{18}O$ and altitude through observations and models. In section 6, we summarize our findings and propose suggestions for future research.

2. DATABASES AND MODELS

[12] To comprehensively review the processes and mechanism of precipitation $\delta^{18}O$, we establish a database, including monitoring stations and ice cores in the TP (section 2.1). We then describe the three models, LMDZiso, ECHAM5-wiso, and REMOiso, used to investigate the mechanisms driving the variability of precipitation $\delta^{18}O$.

2.1. Station $\delta^{18}O$ Database

[13] The precipitation $\delta^{18}O$ monitoring was initiated in the 1980s and has gradually completed as a network of more than 30 observation stations. We have selected event-based precipitation data from 19 observation stations (Figure 1a) of the Tibetan Network for Isotopes in Precipitation (TNIP) and monthly data from 5 observation stations of the GNIP database (GNIP data accessible at http://www.iaea.org/water) which have the most continuous sampling and provide a spatially distributed information over and around the TP (Figure 2). The longest of these records is at Kabul, with monthly based data starting in 1960s. The precipitation data with highest temporal resolution were collected every 3 h near Nagqu from 13 to 27 August 2004. The meteorological parameters from the nearest meteorological stations have also been compiled for comparison with $\delta^{18}O$ data (see section 4). The database was established up to 2007 due to the delays between sampling, measurements, and quality controls.

[14] The station $\delta^{18}O$ database at 24 stations provides $\delta^{18}O$ values at the scale of precipitation events, in addition to monthly and annual values (Figure 2 and Table 1). The data

TABLE 2. Characteristics of the 11 TP Ice Cores[a]

Ice Core	°N	°E	Altitude (m)	Annual Average $\delta^{18}O$ (Period A.D.)	Reference of Ice Core $\delta^{18}O$
East Rongbu	27.15	86.08	6500	−17.5 (1844–1998)	*Hou et al.* [2003a]
Dasuopu	28.38	85.72	7200	−19.88 (1900–1996)	*Yao et al.* [2006b]
Zuoqiupu	29.20	96.92	5500	−13.29 (1956–2006)	*Xu et al.* [2009]
Tanggula 1	33.07	92.08	5800	−15.31 (1940–1990)	*Yao et al.* [1997]
Tanggula 2	33.12	92.08	5743	−13.3 (1935–2004)	*Joswiak et al.* [2010]
Geladandong	33.58	91.18	5720	−12.34 (1935–2004)	*Kang et al.* [2007]
Puruogangri	33.90	89.10	6000	−14.67 (1900–1998)	*Yao et al.* [2006a]
Guliya	35.28	81.48	6200	−14.25 (1900–1992)	*Yao et al.* [1997, 2006b]
Malan	35.83	90.67	5680	−12.58 (1887–1998)	*Wang et al.* [2006]
Dunde	38.10	96.42	5325	−9.93 (1900–1985)	*Yao et al.* [2006b]
Muztagata	38.28	75.10	7010	−16.71 (1955–2003)	*Tian et al.* [2006]

[a]The quality control method for ice core data follows that of *Masson-Delmotte et al.* [2008]. Based on their study, for each location, the database was screened for quality control and a score was attributed, ranging from 0 (minimum quality control) to 4 (maximum quality control). In this study, each of the following four tests contributes one point to the total score: (i) precise $\delta^{18}O$ measurements (analytical uncertainty of 0.2‰ or better), (ii) number of measurements (at least 10 measurements combined to provide interannual variability statistics), (iii) age control on the sampling period, and (iv) seasonal resolution of the measurements.

of Yangcun, Nuxia, Larzi, Dingri, and Zhangmu are only analyzed at the monthly scale due to their short observation period (less than 1 year). Among the 24 stations, 19 TNIP observation stations have been sampled at each precipitation event. Those stations include Taxkorgen, Delingha, Tuotuohe, Yushu, Shiquanhe, Gaize, Nagqu, Yangcun, Bomi, Lulang, Lhasa, Nuxia, Baidi, Larzi, Wengguo, Dingri, Dui, Nyalam, and Zhangmu. The precipitation samples were collected immediately after each precipitation event at each station. Four TNIP stations (including Tuotuohe, Delingha, Lhasa, and Nyalam) and four GNIP stations (Urumqi, Zhangye, Lanzhou, and Kabul) have been sampled for more than 10 years and data are available for interannual variability studies (Figure 2). The TNIP samples collected prior to 2004 were measured using the MAT-252 mass spectrometer from the State Key Laboratory of Cryosphere and Environment, Chinese Academy of Sciences, Lanzhou, with a precision of ±0.2‰, while the samples collected since 2004 have been measured using the MAT-253 mass spectrometer from the Key Laboratory of Tibetan Environment Changes and Land Surface Processes, Chinese Academy of Sciences, Beijing, with an accuracy of ±0.1‰. All the precipitation $\delta^{18}O$ data are reported with respect to the Vienna standard mean ocean water (VSMOW) and represent precipitation amount-weighted values.

[15] The monthly samples collected at TNIP stations were embedded in GNIP (Urumqi, Zhangye, Hetian, Lanzhou, and Kabul) and analyzed at the IAEA Laboratory in Vienna, with an accuracy of ±0.1‰. From the event-based data, monthly, annual, and multiannual $\delta^{18}O$ were calculated, taking into account precipitation weighting.

2.2. Ice Core $\delta^{18}O$ Database

[16] Few meteorological stations exist at very high elevation in the TP. Ice cores allow to complement precipitation sampling for very high elevations. Several ice cores have been recovered in the past 30 years [*Yao and Thompson*, 1992; *Yao et al.*, 1995, 1997, 2006a, 2006b, 2008; *Thompson et al.*, 1997, *Thompson et al.*, 2000; *Hou et al.*, 2003a; *Tian et al.*, 2006; *Wang et al.*, 2006; *Kang et al.*, 2007; *Joswiak et al.*, 2010] over the TP (Figure 1a) with the longest records obtained in the western TP and the shortest ones in the Tanggula Mountains. Here we use 11 ice core records (Table 2) as reference values for the very high elevation where the other data are not available. The $\delta^{18}O$ records from ice cores were measured in different laboratories with varying precisions, better than ±0.2‰, and all the $\delta^{18}O$ records listed in Table 2 have at least annual resolution.

[17] Records of past $\delta^{18}O$ and accumulation rates in TP ice cores have been used to investigate past regional climate variability [*Thompson et al.*, 1989, 2000; *Yao et al.*, 1996a, 1996b, 1999, 2000; *Hou et al.*, 2000, 2002]. Postdepositional processes, which are temporally and spatially variable, can dampen and alter the original precipitation $\delta^{18}O$ signal through melting, sublimation, diffusion, and wind erosion [*Stichler et al.*, 2001; *Schotterer et al.*, 2004]. Melting effect on isotopic signal has been traditionally minimized by drilling ice cores from the regions that experience little or no snowmelt. Ten of our 11 ice cores were recovered from high elevation sites on cold glaciers, without meltwater percolation, while the Zuoqiupu ice core was recovered from a temperate glacier. Among these ice cores, minimal postdepositional modification was estimated for the Dasuopu ice core, considering its high accumulation and the distinct seasonal cycles in chemical species [*Thompson*, 2000]. The consistency of annual $\delta^{18}O$ records from the two Muztagata ice cores [*Tian et al.*, 2006; *Zhao et al.*, 2008] also points to negligible local biases. However, it is impossible to quantify the impact of postdepositional processes on $\delta^{18}O$ and accumulation. We therefore only use their annual averages (see Table 2) as reference values at the ice core sites to extend the vertical coverage for mapping the spatial $\delta^{18}O$ distribution and for discussing altitude effects. The annual average $\delta^{18}O$ value for each ice core in Table 2 is arithmetically calculated based on all the annual $\delta^{18}O$ values for the period listed in the brackets.

2.3. Meteorological Observations and Analyses

[18] The meteorological data (temperature and precipitation amount) from TNIP/GNIP stations are used to analyze the factors impacting on precipitation $\delta^{18}O$ variations in different domains. Temperature and precipitation amount are recorded immediately after each precipitation event

from the TNIP stations. Temperature averages are calculated for monthly/annual analyses, and the corresponding precipitation amounts are calculated as monthly/annual data for each TNIP station. The meteorological data from GNIP stations (downloaded together with corresponding $\delta^{18}O$ data from the website http://www-naweb.iaea.org/napc/ih/GNIP/IHS_GNIP.html) are calculated by the same methods as for the TNIP stations.

[19] For meteorological verification, we use the reanalysis data from the National Center for Environmental Prediction (NCEP)–National Center for Atmospheric Research (NCAR) [*Kalnay et al*., 1996], together with the monthly precipitation data set from the Global Precipitation Climatology Project (GPCP) (http://www.esrl.noaa.gov/psd/). We also refer to monthly values for zonal and meridional winds (at 500 hPa and 850 hPa), as well as sea level pressure from the NCEP/NCAR reanalysis data with a resolution of 2.5° × 2.5°, extracted during the period corresponding to station observations (1958–2007 for the whole study region, 1992–2007 for Delingha, 1991–2005 for Tuotuohe, and 1994–2007 for Lhasa). The GPCP data are from 1979 to 2009 with a resolution of 2.5° × 2.5° for the whole study region.

2.4. Atmospheric Model Simulations

[20] We have selected three isotopic atmospheric circulation models (LMDZiso, REMOiso, and ECHAM5-wiso) that have sufficient spatial resolution to resolve the issues relating to the TP topography. Two of them (LMDZiso and REMOiso) are nudged to atmospheric reanalyses over part of the observation period, to provide a realistic synoptic weather framework. The model outputs (precipitation $\delta^{18}O$, altitude, temperature, and precipitation amount) from the nearest grid points are compared with corresponding observations.

[21] LMDZ is the atmospheric component of the IPSL model and developed at the Laboratoire de Meteorogie Dynamique (LMD). *Risi et al*. [2010b] described the representation of water stable isotopes in LMDZiso and its performances on different time scales for present and past climates. *Gao et al*. [2011] analyzed LMDZiso results by comparison with three station data on the southern TP. They highlighted the importance of both realistic large-scale atmospheric dynamics ensured by nudging to re-analyses, and high spatial resolution for comparison with station data. In this paper, we use two different simulations conducted with LMDZiso: (1) a nudged simulation run from 1979 to 2007 with a resolution of 2.5° latitude × 3.75° longitude (i.e., 277.5 km × 416.25 km), with the boundary conditions similar to those described in *Risi et al*. [2010b]; and (2) a zoomed LMDZiso simulation with the resolution of 50–60 km in a domain extending between 0°N and 55°N in latitude and 60°E and 130°E in longitude, which was run from 2005 to 2007. The three-dimensional fields of the zonal and meridional winds of both simulations were nudged toward those of the ERA-40 reanalyses [*Uppala et al*., 2005] until 2002 and toward those of the operational ECMWF reanalyses thereafter [*Risi et al*., 2010b]. The relaxation time scales are 1 h for the standard simulation, and 1 h (respectively 5 h) for the zoomed simulation outside (respectively inside) the zoomed region. In addition, for numerical stability reasons, the temperature was slightly nudged in the zoomed simulation with time scales of 1 h and 10 days outside and inside the zoomed region, respectively. The nudging is weaker inside the zoomed region to allow for the fine resolution of topographic features to benefit the simulation of the large-scale atmospheric circulation and temperature.

[22] The German Weather Service (DWD-Deutscher Wetterdienst) originally developed the regional circulation model REMO. It was later used to explore climate change by incorporating the physics scheme of the ECHAM4 general circulation model. Then, based on the stable water isotope module of ECHAM4, *Sturm et al*. [2005] embedded the water stable isotopes into REMO. REMOiso proves to reproduce reasonably well climatic and isotopic features across South America, Europe, and Greenland [*Sturm et al*., 2007a, 2007b; *Sjolte et al*., 2011]. The regional REMOiso simulation used here is driven by observed large-scale wind fields using a spectral nudging technique. Winds are nudged toward those simulated by ECHAM, which is itself nudged by ER15 reanalysis. The resolution is 0.5° latitude × 0.5° longitude (~53 km) with 19 vertical hybrid σ-pressure levels, over a 1979–1983 (5 year) time slice.

[23] ECHAM5 is the fifth generation of an atmospheric general circulation model developed at the Max Planck Institute in Hamburg (Germany). ECHAM5 is substantially improved in both the numeric and physics compared to its predecessor ECHAM4, including a flux-form semi-Lagrangian transport scheme, separate prognostic equations for cloud liquid water and cloud ice, a prognostic-statistical cloud cover parameterization, a new cloud microphysical scheme, a mass flux scheme for tropical convection processes with modifications for deep convection, and a new data set of land surface parameters. ECHAM5 successfully simulates the global patterns of surface air temperature and the precipitation amount but overestimates precipitation amount during the Asian summer monsoon season. The water stable isotopes simulations from ECHAM5 (hereafter ECHAM5-wiso) have been run over 10 years with fixed present-day boundary conditions and the horizontal model resolution is 0.75° latitude × 0.75° longitude in T159 spectral mode. The global performance of ECHAM5-wiso was previously assessed with respect to spatial and seasonal GNIP data. Note that this ECHAM5-wiso simulation was run without nudging to reanalyses and therefore can only be compared with the mean seasonal cycle of observations.

3. IMPACT OF THE WESTERLIES AND INDIAN MONSOON ON SPATIAL AND TEMPORAL PATTERNS OF PRECIPITATION $\delta^{18}O$

3.1. Observed Spatial and Temporal Characteristics of Precipitation $\delta^{18}O$

[24] Three different seasonal patterns from the observed TP precipitation $\delta^{18}O$ in different TP regions are shown in Figure 3: (1) minimum $\delta^{18}O$ in winter and maximum $\delta^{18}O$ in summer, associated with high precipitation and temperature in summer (Figures 3a–3c); (2) maximum $\delta^{18}O$ in late

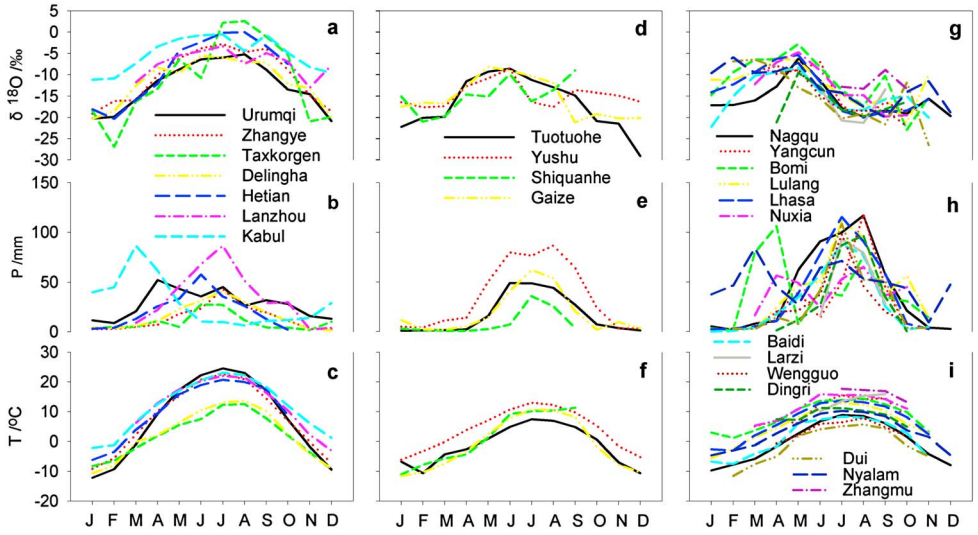

Figure 3. Seasonal patterns of observed precipitation $\delta^{18}O$, precipitation amount (P), and temperature (T) in different TP domains. (a) Monthly weighted $\delta^{18}O$ (‰), (b) precipitation amount (mm/month), and (c) temperature averages (°C) in the westerlies domain (seven stations). (d–f) Same as Figures 3a–3c but for the transition domain (four stations). (g–i) Same as Figures 3a–3c but for the monsoon domain (13 stations). For each station, data are averaged over observation periods (see Table 1 and Figure 2 for details).

winter/early spring and minimum $\delta^{18}O$ in late summer (more than 10‰ of seasonal amplitude for multiyear averaged data; Figure 3g), associated with a maximum temperature in summer (Figure 3i) and a precipitation pattern with distinctive two peaks with one in early spring and one in summer (Figure 3h); and (3) seasonal pattern of $\delta^{18}O$ is complex and no clear extrema either for winter or summer (Figure 3d), with precipitation and temperature showing small maxima in summer (Figures 3e and 3f). We examine these patterns using reanalysis data (section 3.3.1) and models (section 3.3.2). The stations with enriched summer $\delta^{18}O$ (Figure 3a) correspond to the region, north of 35°N, dominated by the westerlies (hereafter "the westerlies domain"), and depict a close link between $\delta^{18}O$ and local temperature and weak relationships with precipitation amount (see section 4). The stations with clear summer depletion (Figure 3g) correspond to the monsoon region, south of 30°N, dominated by the Indian monsoon (hereafter "monsoon domain"), showing an antiphase between $\delta^{18}O$ and precipitation amount (Figures 3g and 3h). The regions where seasonal cycles show more complicated $\delta^{18}O$ variations (Figure 3d, located between 30°N and 35°N) are defined as the transition domain, suggesting shifting influences between the westerlies and Indian monsoon. This regional classification based on seasonal patterns of precipitation $\delta^{18}O$ (Figures 3a, 3d, and 3g) is consistent with climatic zones defined by the spatial distribution of annual and June-July-August (JJA) temperature, precipitation, and wind fields (Figure 4).

[25] Figure 3g shows a unique feature characterized by abrupt depletion of precipitation $\delta^{18}O$ around May and by the most depleted $\delta^{18}O$ value around August in the monsoon domain. Previous study found that Bay of Bengal (BOB) acts as the major moisture source for the abrupt depletion of precipitation $\delta^{18}O$ in early May in the southeastern TP [*Yang et al*., 2012]. After the BOB monsoon establishment, the Indian monsoon from the southern Indian Ocean develops [*Joseph et al*., 2006; *Wang et al*., 2009], which might be another major moisture source leading to most depleted precipitation $\delta^{18}O$ around August.

[26] We now briefly describe the large spatial gradients arising from these distinct patterns. Summer precipitation is maximum in the Bay of Bengal (BOB) and decreases northward in the TP (Figure 4b) with an annual gradient of −23.28 mm/°N ($R=-0.41$, $p>0.1$), and strong differences between the JJA gradient, −11.21 mm/°N ($R=-0.60$, $p>0.1$), and the December-January-February (DJF) gradient, 0.25 mm/°N ($R=0.03$, $p>0.1$). Annual average temperatures at 24 precipitation stations (Figure 4d) show a linear decrease with latitude by 0.34°C/°N ($R=0.34$, $p>0.1$). Temperature gradient is larger (0.73°C/°N, $R=0.57$, $p>0.1$) in JJA and smaller (−0.25°C/°N, $R=0.28$, $p>0.1$) in DJF. In summer, the southern TP is characterized by strong southerlies and southwesterlies at 500 hPa, which gradually weakens from 30°N to 35°N before turning into the prevailing westerlies to the north of 35°N (Figure 4k). In winter, the westerlies prevail over the whole TP (Figure 4l), without obvious variation of precipitation from south to north (Figures 4c and 4l). Precipitation $\delta^{18}O$ generally increases northward (Figure 4g) at a rate of 0.69‰/°N ($R=0.64$, $p<0.01$, $n=35$). Spatial gradients appear more pronounced in JJA (1.2‰/°N, $R=0.82$) than in DJF (−0.52‰/°N, $R=-0.54$). The spatial changes of precipitation $\delta^{18}O$ in different seasons, particularly that of the JJA $\delta^{18}O$ (Figure 4h), clearly depict the spatial pattern of summer precipitation (Figures 4b and 4k) associated with depleted annual $\delta^{18}O$ (<−10‰) (Figure 4g). This emphasizes the influence of the Indian monsoon [*Tian et al*., 2003] and thus motivates further investigations of the relationships between precipitation $\delta^{18}O$ and moisture origin in section 3.3.

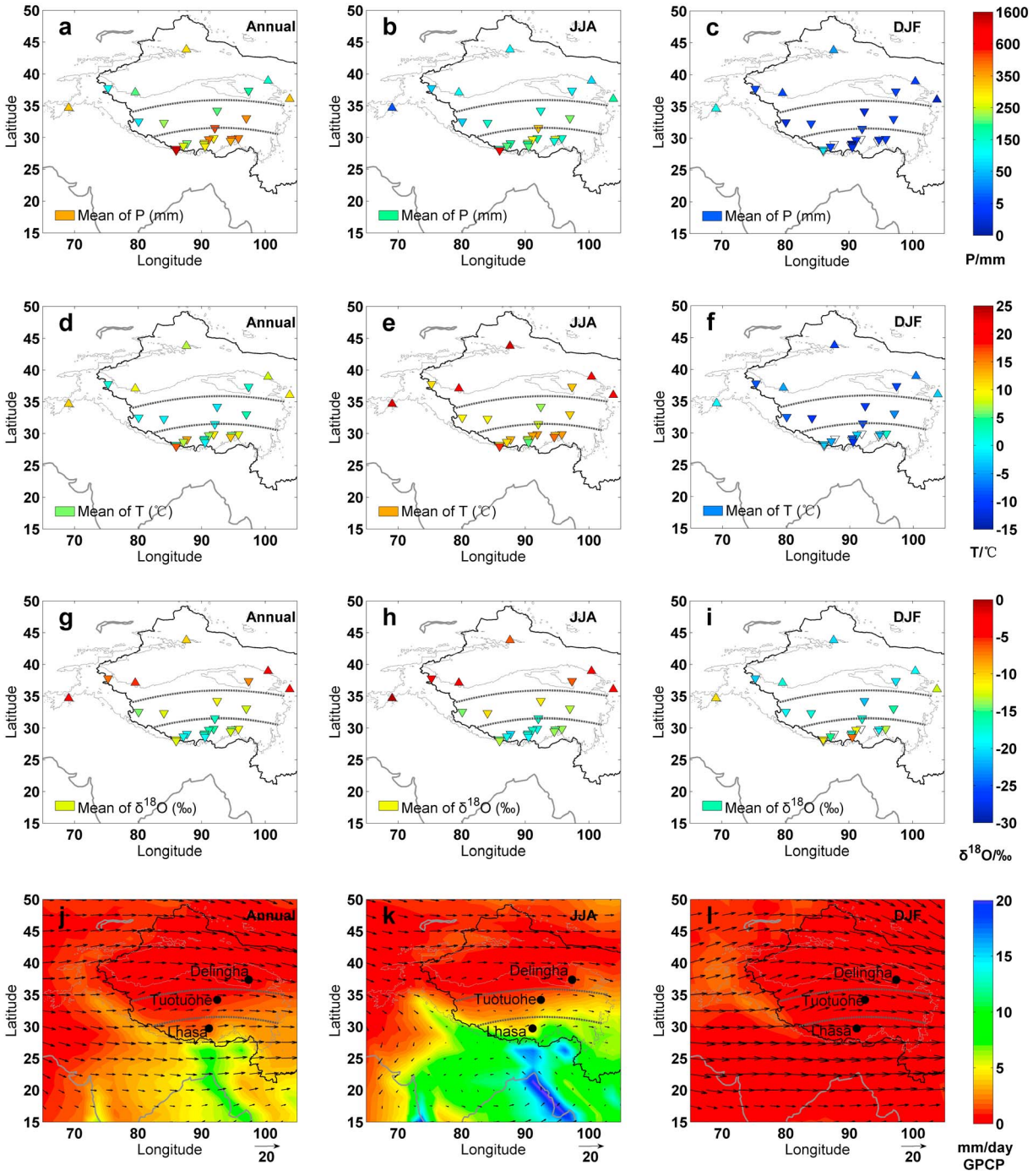

Figure 4. Spatial patterns of annual precipitation amount, temperature, and precipitation $\delta^{18}O$ at precipitation stations, and the wind fields together with precipitation amount over the TP and surrounding regions. (a) Long-term averaged annual precipitation amount (mm) (triangles). (b and c) Same as Figure 4a but for JJA and DJF (triangles). (d) Long-term averaged annual temperature (°C). (e and f) Same as Figure 4d but for JJA and DJF. (g) Long-term averaged annual precipitation $\delta^{18}O$. (h and i) Same as Figure 4g but for JJA and DJF. (j) Composite of the annual mean wind fields (arrows) superimposed on the annual precipitation (mm/d, shading). (k and l) Same as Figure 4j but for JJA and DJF. Wind field data at 500 hPa are from the NCEP/NCAR reanalysis data (averaged from 1958 to 2007), and precipitation data are from the Global Precipitation Climatology Project (GPCP; http://www.esrl.noaa.gov/psd/data/gridded/data.gpcp.html), averaged from 1979 to 2009. Up triangles stand for GNIP stations and down triangles for TNIP stations. The grey line shows the boundary where the elevation is above 3000 m. The dashed lines show the schematic boundaries separating the three domains (the westerlies domain, the transition domain, and the monsoon domain).

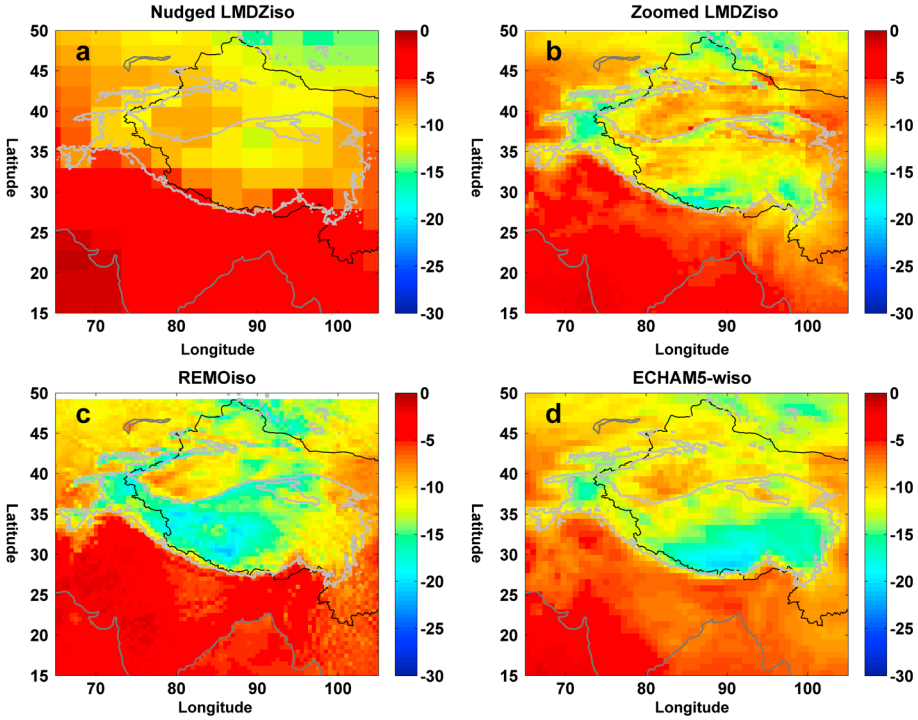

Figure 5. Annual precipitation $\delta^{18}O$ (‰) simulated by (a) nudged LMDZiso, (b) zoomed LMDZiso, (c) REMOiso, and (d) ECHAM5-wiso. The grey line shows the contour where elevation is above 3000 m. Different models were run for different periods (see Table 3).

3.2. Simulations of Spatial and Temporal Patterns

[27] Figure 5 shows the spatial distribution of annual precipitation $\delta^{18}O$ in the TP from the nudged LMDZiso (Figure 5a), zoomed LMDZiso (Figure 5b), REMOiso (Figure 5c), and ECHAM5-wiso (Figure 5d) simulations. The spatial patterns from the three simulations with high spatial resolution (zoomed LMDZiso, REMOiso, and ECHAM5-wiso) appear more consistent with the observations shown in Figure 4g. In the following sections, we will therefore focus on the results of the three high-resolution simulations.

[28] The models distinguish the difference between the westerlies and Indian monsoon. In the northern TP, zoomed LMDZiso and ECHAM5-wiso correctly reproduce the spatial distribution of $\delta^{18}O$ with the highest $\delta^{18}O$ values in the northwest and northeast TP (Figures 5b and 5d). The patterns of precipitation $\delta^{18}O$ simulated by ECHAM5-wiso and zoomed LMDZiso are quite similar for regions to the south of 35°N ($R = 0.82$, $p < 0.01$). The lowest $\delta^{18}O$ is correctly simulated in the southern TP along the Himalayas, although the results of ECHAM5-wiso are about 2‰ lower than zoomed LMDZiso and observations. This means that zoomed LMDZiso is better in capturing the magnitude and north-south patterns of precipitation $\delta^{18}O$.

[29] The three models show different abilities to reproduce the seasonal patterns of precipitation $\delta^{18}O$, precipitation amount, and temperature in the three domains and perform better in the westerlies domain than the other ones (Figure 6). Compared with the observed data, they can successfully reproduce the unimodal variation of $\delta^{18}O$ (high values in summer and low values in winter) in the westerlies domain (Figure 6a), the highest $\delta^{18}O$ in June and subsequent decrease in the transition domain (Figure 6d), and the bimodal variation of $\delta^{18}O$ in the monsoon domain (Figure 6g). The best simulations of seasonal precipitation $\delta^{18}O$ are obtained from zoomed LMDZiso, especially in the westerlies and monsoon domains. Zoomed LMDZiso captures the seasonal variation of precipitation amount in the three domains (Figures 6b, 6e, and 6h), although all the models fail to simulate precipitation amount with large deviations. The three models reproduce the seasonal pattern of temperature better than that of precipitation amount, with systematic underestimation in the three domains (Figures 6c, 6f, and 6i). In the westerlies domain, the drier bias is consistent with the well-known bias over midlatitude continents in summer [*Klein et al.*, 2006; *Cheruy et al.*, 2012], associated with a land-atmosphere feedback in which drier soils dissipate more heat through sensible heat flux rather than latent heat flux. The wetter and cooler bias in the monsoon domain is a common feature of atmospheric and coupled general circulation models [*Su et al.*, 2013] and may be associated with the cooling effect of the overestimated cloud cover from the overestimated precipitation. In summary, the simulation from zoomed LMDZiso fits observations better, compared with those of REMOiso and ECHAM5-wiso.

3.3. Atmospheric Circulation Processes Controlling Precipitation $\delta^{18}O$

3.3.1. Associations of Precipitation $\delta^{18}O$ With Sea Level Pressure, Wind Fields, and Convection Based On Observations

[30] In this section, we have selected three stations with long $\delta^{18}O$ records (Delingha, Tuotuohe, and Lhasa) as representative of each domain. In order to assess the relationships between seasonal precipitation $\delta^{18}O$ and large-scale atmospheric circulation, we have calculated the linear correlation

TABLE 3. Specifications of the Simulations Used in the Paper

Models	Resolution	Mean Number of Grid Points on the TP	Period	Nudging Method	Reference
Standard LMDZiso	2.5° × 2.5°	63	1979–2007	ERA-40 reanalyses and ECMWF reanalyses	*Risi et al.* [2010b] and *Gao et al.* [2011]
Zoomed LMDZiso	~50 km	1472	2005–2007	ERA-40 reanalyses and ECMWF reanalyses	*Risi et al.* [2010a] and *Gao et al.* [2011]
REMOiso	0.5° × 0.5°	1800	1979–1983	ERA15 and spectral nudging	*Sturm et al.* [2005, 2007a, 2007b]
ECHAM5-wiso	0.75° × 0.75°	861	10 years	Climatological control simulation	*Werner et al.* [2011]

coefficients between precipitation $\delta^{18}O$ at each station and sea level pressure (SLP) and meridional and zonal wind fields for JJA and DJF (Figure 7).

[31] Our analysis shows that $\delta^{18}O$ at Delingha is negatively correlated with SLP over the BOB and Arabian Sea (AS) in winter (DJF) and positively correlated with the SLP over the BOB and AS in summer (JJA) (Figures 7a and 7d). But the correlations with wind fields and SLP are the weakest ($R < 0.2$) at Delingha. This confirms earlier studies that this region is hardly influenced by the Indian monsoon [*Tian et al.*, 2001b; *Li et al.*, 2006].

[32] The precipitation $\delta^{18}O$ is negatively correlated with the SLP over the BOB and AS in winter at both Tuotuohe and Lhasa (Figures 7e and 7f), where the strongest correlations ($R = \sim 0.8$) are obtained with wind fields (figures not shown). In summer, the correlation with SLP is positive at Tuotuohe (Figure 7b) and negative at Lhasa (Figure 7c). This suggests a more systematic impact of the Indian monsoon on precipitation $\delta^{18}O$ at Lhasa than Tuotuohe and to the fact that Tuotuohe is in the intersection of the shifting influences between the westerlies and Indian monsoon.

3.3.2. Moisture Origin of Precipitation $\delta^{18}O$ Based On Simulations

[33] We now take advantage of the model framework to analyze the moisture transport based on REMOiso and zoomed LMDZiso as diagnosed by horizontal water vapor advection that is vertically integrated over the entire atmospheric column (i.e., surface to top 100 hPa) and by water tagging, respectively. In REMOiso, DJF moisture is transported by the westerlies (Figure 8), which might result in the marked west-east and northward precipitation $\delta^{18}O$ gradient. A strong latitudinal effect is also simulated, with high $\delta^{18}O$ values south of the Himalayas and a decrease of $\delta^{18}O$ as latitude increases. In summer, the REMOiso simulation shows a horizontal water

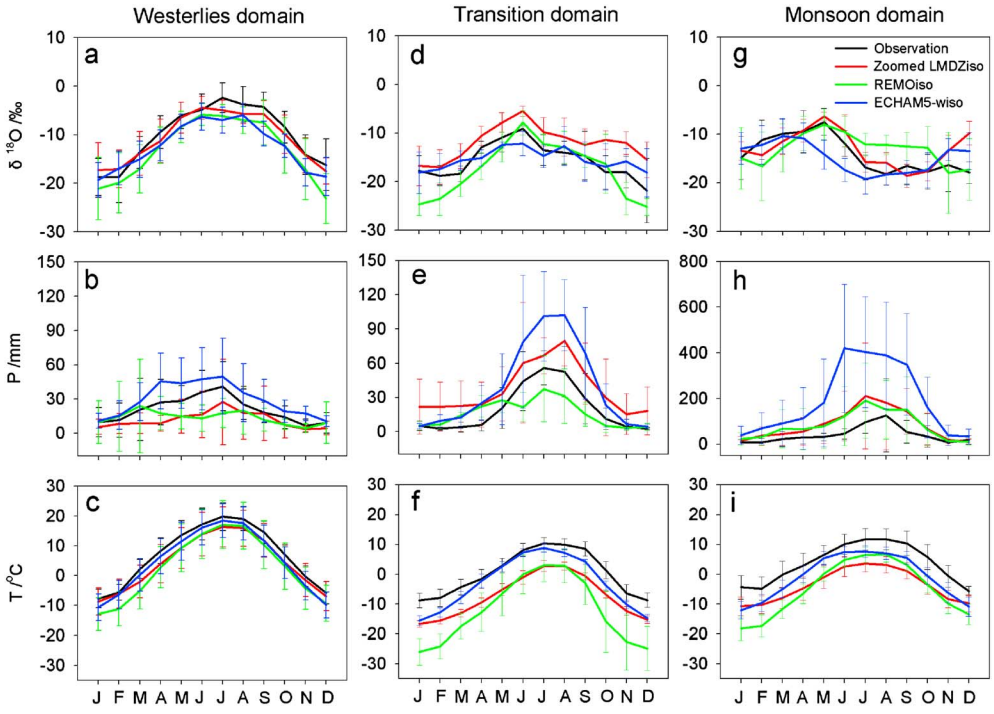

Figure 6. Seasonal patterns of averaged precipitation $\delta^{18}O$, precipitation amount, and temperature from observations (black), zoomed LMDZiso (red), REMOiso (green), and ECHAM5-wiso (blue) in different TP domains. (a) Weighted monthly $\delta^{18}O$ (‰), (b) precipitation amount (mm/month), and (c) temperature (°C) averaged from seven stations in the westerlies domain. (d–f) Same as Figures 6a–6c but for the transition domain, averaged from four stations. (g–i) Same as Figures 6a–6c but for the monsoon domain, averaged from 13 stations.

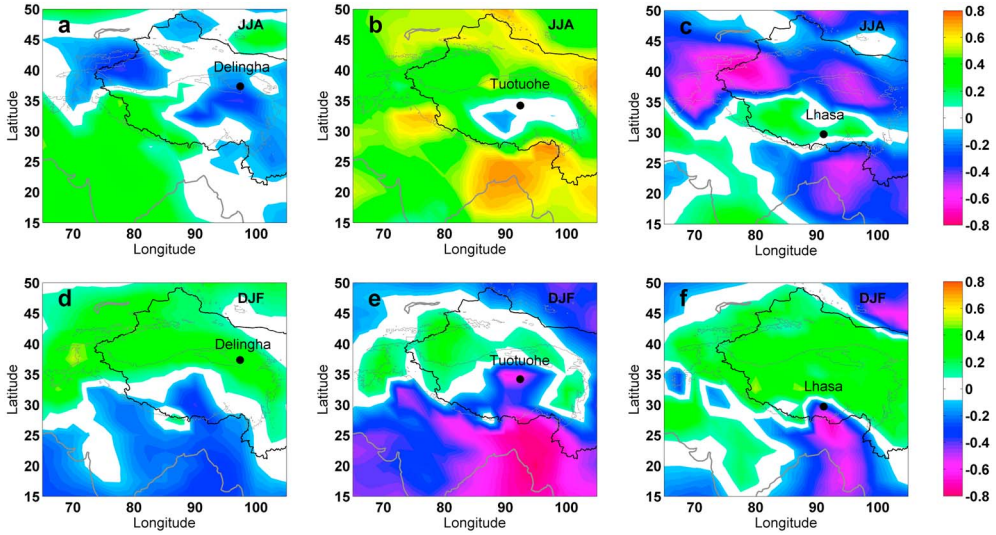

Figure 7. Correlations of summer (JJA) precipitation $\delta^{18}O$ with SLP (shading) at 850 hPa: (a) Delingha during the period 1992–2007, (b) Tuotuohe during the period 1991–2005, and (c) Lhasa during the period 1994–2007; (d–f) same as Figures 7a–7c but for winter (DJF). SLP data are downloaded from NCEP/NCAR reanalyses. Correlations were calculated online from http://www.esrl.noaa.gov/psd/cgi-bin/data/getpage.pl without additional significant test.

vapor transportation driven by strong winds from the Arabian Sea and the BOB to the TP (Figure 8). The highest precipitation $\delta^{18}O$ values are encountered in the Arabian Sea, leading to a strong west-east gradient south of 30°N in JJA, and minimum $\delta^{18}O$ values along the Himalayas. Observations of the spatial gradients of $\delta^{18}O$ in JJA and DJF, combined with moisture transport analyses, demonstrate the impact of large-scale moisture advection. The exact moisture sources can be

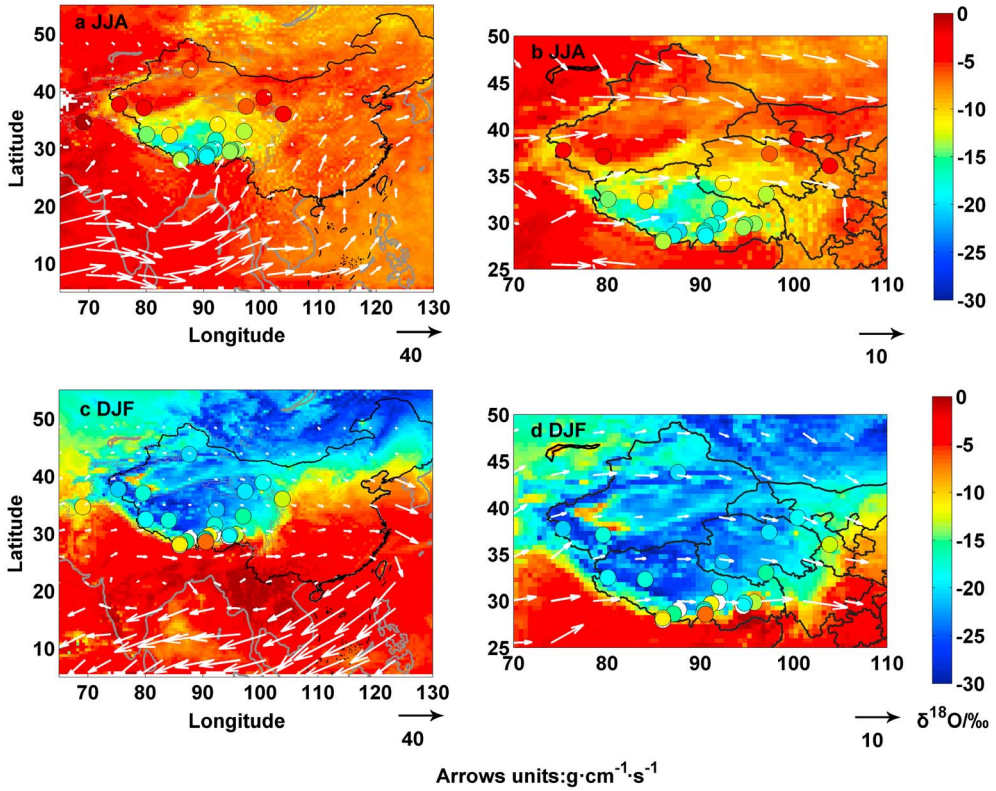

Figure 8. Averaged precipitation $\delta^{18}O$ for (a, b) JJA and (c, d) DJF simulated by REMOiso, with zoomed results over the TP. Shadings represent simulated precipitation $\delta^{18}O$, and arrows represent the horizontal water vapor transport (in g cm^{-1} s^{-1}) that is vertically integrated over the entire atmospheric column (i.e., surface to top layer = 100 hPa). Average precipitation $\delta^{18}O$ values at TP stations are displayed with colored dots.

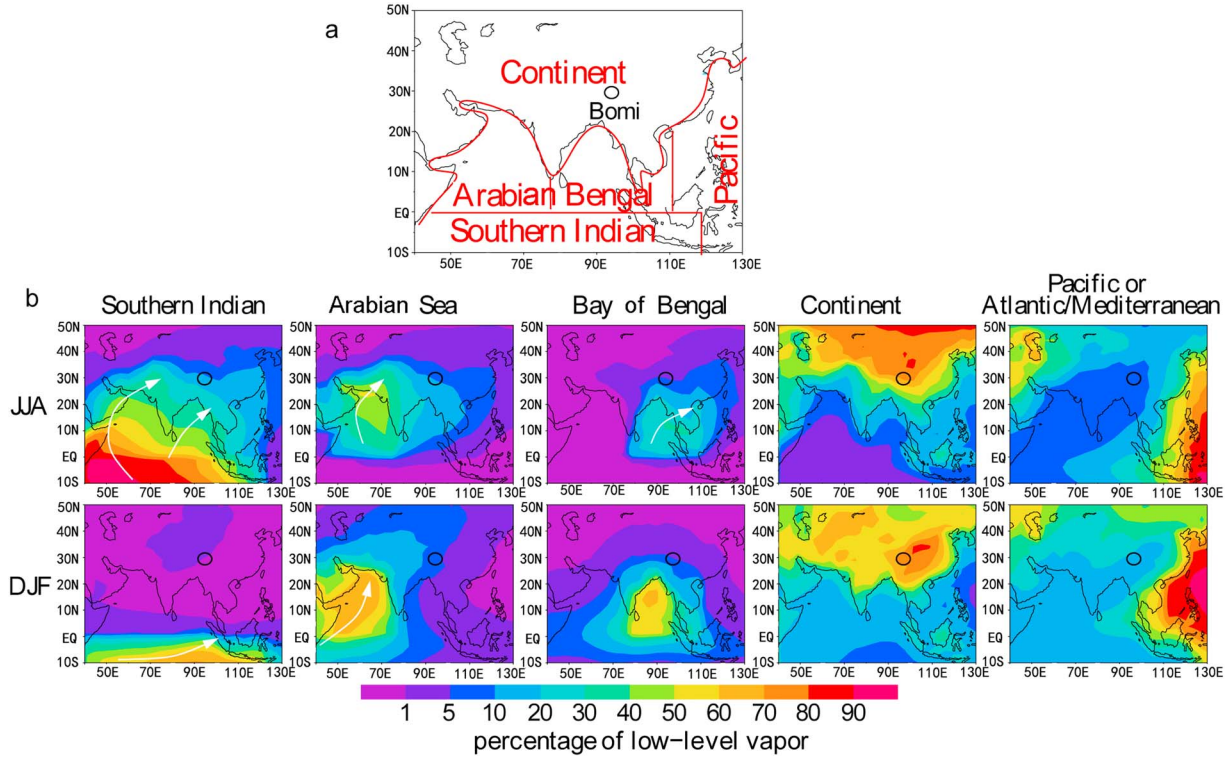

Figure 9. Water tagging experiment conducted using the zoomed LMDZiso model. (a) Definition of evaporative regions for water tagging. (b) Proportion of the JJA and DJF vapor originating from these different evaporative sources. The white arrows are an idealized representation of the dominant moisture flow. The open circle is a monitoring station in the TP (Bomi).

further investigated using water tagging, as implemented in zoomed LMDZiso.

[34] Water tagging is a method used to quantify different moisture contributions from continental and oceanic evaporation sources and is available in the zoomed LMDZiso 2005–2007 simulations. Five potential moisture sources are considered: (1) continental sources, (2) Arabian Sea, (3) Bay of Bengal, (4) southern Indian Ocean, and (5) Pacific, Atlantic, or Mediterranean sources (Figure 9a). Continental recycling is one of the main moisture sources in the TP during both winter and summer. The contribution from the Pacific, Atlantic, and Mediterranean sources is significant in winter. The moisture sources shift to the BOB and Arabian Sea in April and to the Arabian Sea in May and June. In summer, the dominant moisture source is the southern Indian Ocean, once the advection of moisture by monsoon is well established (Figure 9b). This shift in moisture sources explains the $\delta^{18}O$ depletion observed during the monsoon season.

[35] Marine air masses transported from the southwest cannot directly reach the northern TP [*Tian et al.*, 2001a], where continental recycling enhanced by evaporation over the land surface is significant and enriches summer precipitation $\delta^{18}O$ [*Tian et al.*, 2001b; *Yu et al.*, 2006a, 2007]. Water tagging quantifies the effect of continental recycling on meridional gradients and seasonality over the TP. In the northern TP, zoomed LMDZiso produced maximum continental recycling in summer which contributes to the enriched precipitation $\delta^{18}O$. Zoomed LMDZiso shows that continental recycling amplifies the $\delta^{18}O$ seasonal cycle by 15% at Delingha.

[36] Both the REMOiso and zoomed LMDZiso models clearly depict close links between seasonal variations of $\delta^{18}O$ and the moisture sources and transport paths. They produce depleted summer $\delta^{18}O$ in the southern TP, which resulted from intense convection of oceanic moisture during transportation to the TP. This confirms the earlier interpretation of observations based on atmospheric trajectory analyses [*Tian et al.*, 2007]. The water tagging diagnostics confirm the information derived from moisture advection and further emphasize the importance of continental recycling on the magnitude of seasonal $\delta^{18}O$ variations.

4. RELATIONSHIPS OF PRECIPITATION $\delta^{18}O$ WITH TEMPERATURE AND PRECIPITATION AMOUNT

4.1. Observed Characteristics of Temperature and Precipitation Amount Effects

[37] Three stations, Delingha, Tuotuohe, and Lhasa, are selected to discuss the event-based relationships between precipitation $\delta^{18}O$ and temperature/precipitation amount in different domains (Figure 10). The lengths of observations at these three stations are 15 years for Delingha, 13 years for Tuotuohe, and 12 years for Lhasa.

[38] In the westerlies domain, the variation of the daily precipitation $\delta^{18}O$ coincides with temperature variation ($R = 0.80$, $p < 0.01$, $n = 219$), with the highest $\delta^{18}O$ values (as high as −1.16‰) in summer and lowest values (as low as −35.61‰) in winter (Figure 10a). In the transition domain, $\delta^{18}O$ mainly varies with temperature, except a large shift between days 200 and 300 related to intensifying

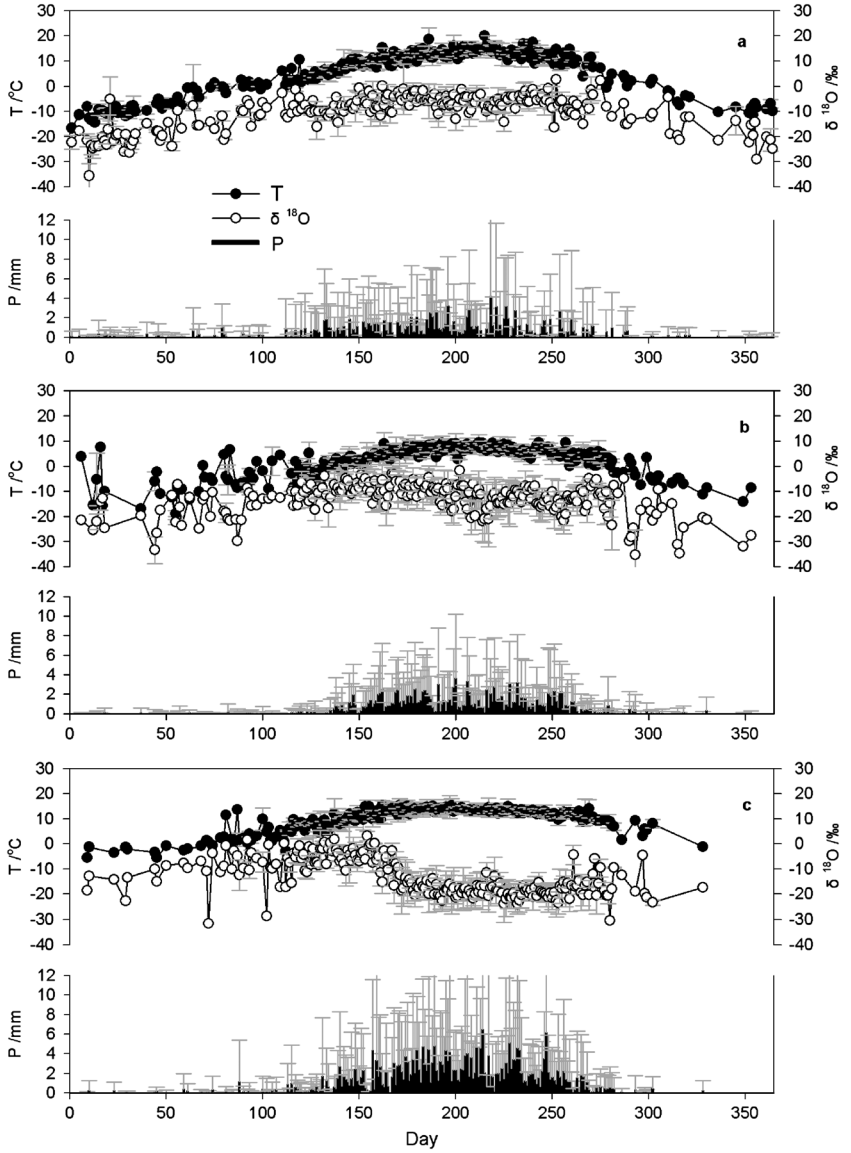

Figure 10. Observed daily changes of precipitation $\delta^{18}O$, temperature, and precipitation amount based on event sampling at (a) Delingha (15 years), (b) Tuotuohe (13 years), and (c) Lhasa (12 years). The error bar is calculated from interannual variations.

precipitation (Figure 10b). In the monsoon domain, $\delta^{18}O$ undergoes a remarkable depletion from around day 150 and remains low until day 300 (Figure 10c), which is obviously related to changes in precipitation rather than temperature. The relationship between precipitation $\delta^{18}O$ and precipitation amount is complex. In winter when the westerlies prevail, the higher $\delta^{18}O$ values concur with low precipitation amount. By contrast, during the whole summer monsoon season, $\delta^{18}O$ is depleted for events with high precipitation amount. An abrupt decrease of $\delta^{18}O$ corresponds to the abrupt increase of precipitation amount from day 154 to day 167 (Figure 10c), which reflects the shift from the westerlies to the Indian monsoon, with different histories of convection and precipitation along air mass trajectories [*Vimeux et al.*, 2005]. The most depleted precipitation $\delta^{18}O$ occurs from day 225 to day 253, indicating the impact of the mature Indian monsoon. From multiyear statistics (Figures 10a–10c), our data depict quite stable temperatures compared to the larger variabilities in precipitation amount and $\delta^{18}O$. The most obvious case of such variability is shown from day 202 (−4.89‰) to day 203 (−27.80‰) in the transition domain (Figure 10b).

[39] There are a larger positive slope and a stronger correlation coefficient between daily $\delta^{18}O$ and temperature at Delingha (0.62‰/°C, $R = 0.74$; Figure 11a) than Tuotuohe (0.23‰/°C, $R = 0.16$; Figure 11b), while the slope and correlation coefficient are negative at Lhasa (−0.31‰/°C, $R = -0.16$; Figure 11c). Similar patterns are observed, and the correlations have been clearly improved for all those three stations at the monthly scale (Figures 11e–11g).

[40] The same analysis is done for the precipitation amount effect at the three stations (Figure 12). At the daily scale, there is a negative correlation between $\delta^{18}O$ and precipitation amount at all those three stations (Figures 12a–12c), with the largest slope (−0.37‰/mm) and strongest correlation ($R = -0.26$, $p < 0.01$) at Lhasa (Figure 12c). At the monthly

scale, however, the negative correlation turns into positive at both Delingha (Figure 12e) and Tuotuohe (Figure 12f), whereas the negative correlation between $\delta^{18}O$ and precipitation amount remains ($R = -0.32$, $p < 0.01$) at Lhasa (Figure 12g). Earlier studies [*Tian et al*., 2003; *Yu et al*., 2007] have also reported similar amount effect in the southern TP (−0.27‰/mm) [*Liu et al*., 2007]. The depletion in the southern TP is associated with the large scale Indian monsoon flow undergoing intense convection in tropical storms where an ensemble of physical and microphysical processes functions in the convective system [*Risi et al*., 2008b].

[41] Since the shifting influence between the westerlies and Indian monsoon is an intraseasonal characteristic over the TP all year round, we detect the different relationships of precipitation $\delta^{18}O$ with temperature and precipitation amount in the westerlies dominant winter season, referred to as westerly season, and in the Indian monsoon dominant summer season, referred to as monsoon season.

[42] Remarkable temperature effect is identified in the three domains in the monsoon season (Figures 13a–13c) and the westerly season (Figures 13e–13g). The largest slope of 0.80‰/°C during westerly season in the westerlies domain ($R = 0.69$, $p < 0.01$) is close to the global average (0.69‰/°C) [Dansgaard, 1964], while others change from 0.14‰/°C to 0.26‰/°C comparable to the range of slopes (0.17‰/°C–0.76‰/°C) identified in previous studies [*Yao et al*., 1996b; *Tian et al*., 1997; *Yu et al*., 2006b, 2008]. Stations in the westerlies domain show the best positive correlation between $\delta^{18}O$ and temperature (Figures 13a and 13e).

[43] The above discussion highlights the existence of significant temperature effect when either the westerlies or Indian monsoon is the sole dominant atmospheric process. It indicates that the mechanism of temperature effect revealed for the East Asian monsoon region [*Yang et al*., 2011] is also functioning in the Indian monsoon region. Thus, data length, time scales, and atmospheric circulations must be cautiously considered since they may result in different conclusions.

4.2. Simulations of Temperature and Precipitation Amount Effects

[44] We restrict this analysis to the nudged simulations (zoomed LMDZiso and REMOiso) which are forced to represent realistically the variability of large-scale atmospheric circulation.

[45] Significantly positive correlations between daily $\delta^{18}O$ and temperature are simulated in the westerlies domain (Figure 11d), comparable with our database (see previous section). However, both models overestimate the temperature control (correlation and slope) in the transition domain (Figure 11d). In the monsoon domain, zoomed LMDZiso and REMOiso display an unrealistic positive correlation with temperature ($R = 0.17$ and $R = 0.46$, respectively).

[46] At the monthly scale, the two models produce results comparable with observations in the westerlies and transition domains, but again produce results of opposite signs with respect to data in the monsoon domain (Figure 11h). The correlations between precipitation $\delta^{18}O$ and temperature are visibly improved at the monthly scale. This indicates that the models can correctly capture the regional characteristics, thus posing a potential to represent some physical processes relating to large scale atmospheric circulations. Due to the shortness of the simulations, it is not possible to explore the interannual and longer time scales.

[47] At the event scale, both models display significantly negative correlations between daily precipitation $\delta^{18}O$ and precipitation amount in the monsoon domain ($R = -0.43$ from zoomed LMDZiso and $R = -0.26$ from REMOiso, p 0.01) (Figure 12d), consistent with observations. However, they show unrealistic positive relationships between daily precipitation $\delta^{18}O$ and precipitation amount in the westerlies and transition domains, inconsistent with observations. At the monthly scale, the models simulate positive correlations between precipitation $\delta^{18}O$ and precipitation amount in the transition and westerlies domains, consistent with observations (Figure 12h). In the monsoon domain, the negative correlation is overestimated from zoomed LMDZiso, but a positive correlation simulated from REMOiso is opposite to observations (Figure 12h). We conclude that models have caveats for the representation of climate-$\delta^{18}O$ relationships in the TP, especially at the event basis. We also note that from the daily to monthly scales, the relationships between precipitation amount and $\delta^{18}O$ appear weak both in observations and models in the monsoon domain.

[48] The simulated relationships between precipitation $\delta^{18}O$ and temperature remarkably coincide with observations (Figures 13d and 13h), when we separately considered the monthly data with respect to the monsoon and westerly seasons. All the models reproduce the positive correlations in monsoon season at the three domains with a reasonable range from 0.20 to 0.87. Although the simulated slope from zoomed LMDZiso in the monsoon domain (0.88) is much larger than the observed result, it is still close to the previous observed ranges (from 0.17 to 0.76) [*Yao et al*., 1996; *Yu et al*., 2006a]. The lowest simulated slope (0.03) from REMOiso exists in the transition domain during monsoon season, which is identified from the dew point [*Yu et al*., 2006b], indicating the error of the temperature parameterization in the model. Except the transition domain, all the models successfully simulate the positive correlations in westerly season, and the strongest correlation exists during westerly season in the westerlies domain. The different performances of models in the westerlies and monsoon domain could be due to an underestimation of the variability linked with continental recycling. This demonstrates that all the models succeed in the main processes and control factor of precipitation $\delta^{18}O$, and the differences between previous observations and simulations at intraseasonal scale may be resulted from the inadequate observation.

5. IMPACT OF THE WESTERLIES AND INDIAN MONSOON ON THE RELATIONSHIP BETWEEN PRECIPITATION $\delta^{18}O$ AND ALTITUDE EFFECT

5.1. Observed Altitudinal Lapse Rates

[49] With a wide altitude variation from 900 m to over 7000 m, our data compilation enables a comprehensive study

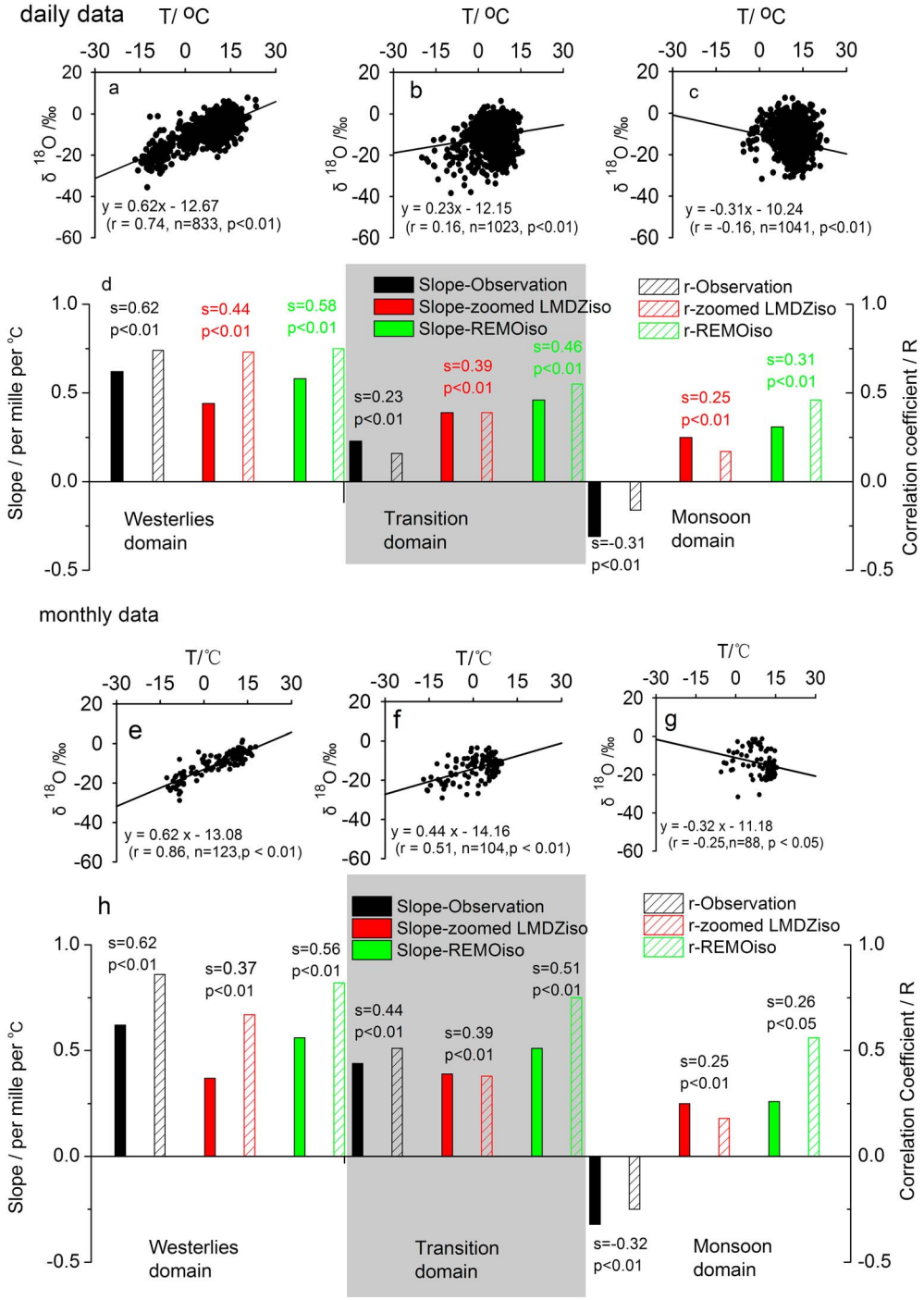

Figure 11. Regressions of observed precipitation $\delta^{18}O$ with temperature based on daily and monthly data, and corresponding simulated slopes and correlation coefficients for daily and monthly data at (a, e) Delingha, (b, f) Tuotuohe, and (c, g) Lhasa, representing the corresponding three domains. Figures 11a–11c are the regressions between $\delta^{18}O$ and temperature based on daily data; (d) comparisons between the simulated and observed slopes and correlation coefficients in the three domains. Figures 11e–11g are the same as Figures 11a–11c but for monthly data. "s" stands for slopes and "p" for the significance level of a Pearson test.

of the altitude effect of precipitation $\delta^{18}O$ over the TP. We have conducted this analysis for the three domains (westerlies, transition, and monsoon) using both the station and the ice core data. As shown in Figure 14a, the observed lapse rate is larger in the westerlies domain (0.17‰/100 m) than that in the monsoon domain (0.13‰/100 m), while the observed lapse rate is smallest in the transition domain (0.06‰/100 m, insignificant correlation). The loss of clear altitude effect in the transition domain is consistent with previous studies reporting significant altitude effect in regions dominated by a single moisture source [*Kurita et al.*, 2005; *Yang et al.*, 2009].

[50] In the westerlies domain, the geographical controls on precipitation $\delta^{18}O$ are best expressed by a multiple linear

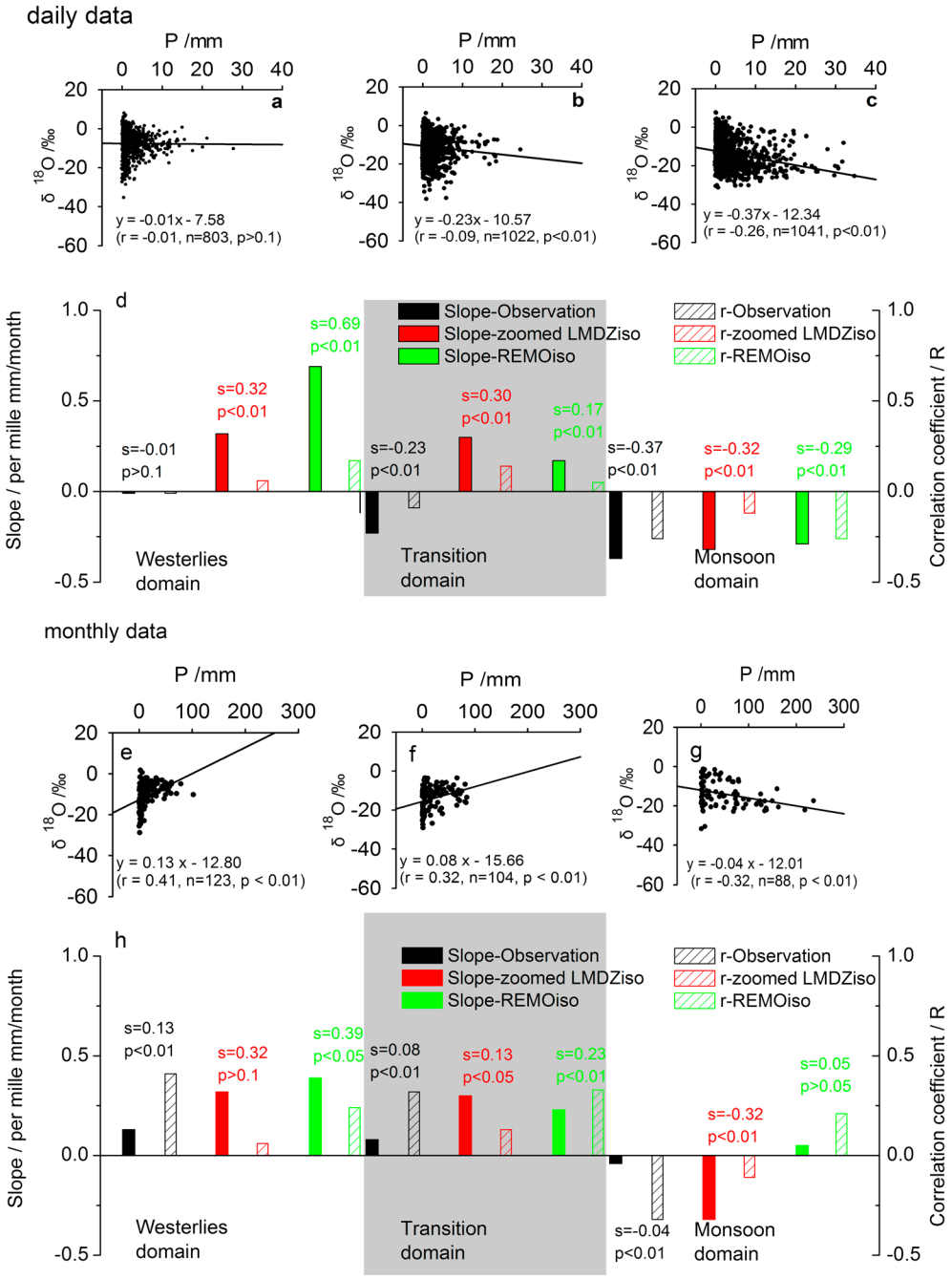

Figure 12. Regressions of observed precipitation $\delta^{18}O$ with precipitation amount based on daily and monthly data, and corresponding simulated slopes and correlation coefficients for daily and monthly data at (a, e) Delingha, (b, f) Tuotuohe, and (c, g) Lhasa, representing the corresponding three domains. Figures 12a–12c are the regressions between $\delta^{18}O$ and precipitation amount based on daily data; (d, h) comparisons between the simulated and observed slopes and correlation coefficients in the three domains. Figures 12e–12h are the same as Figures 12a–12d but for monthly data. "s" stands for slopes and "p" for the significance level of a Pearson test.

regression including altitude (Alt, in meters above sea level (asl)) and latitude (°N):

$$\delta^{18}O = -0.002 \times \text{Altitude} + (-0.74) \times \text{Latitude} + 25.767 \ (R = 0.95, p < 0.01).$$

[51] In the monsoon domain, a stepwise linear regression of $\delta^{18}O$ with spatial parameters (longitude, latitude, and altitude) shows the altitude as the only significant factor. The best model accounting for monsoon $\delta^{18}O$ variation includes both altitude and precipitation amount:

$$\delta^{18}O = (-0.002) \times \text{Altitude} + 0.003 \times P - 9.873 (R = 0.84, p < 0.05),$$

where P is the precipitation amount (mm/yr). The drivers of

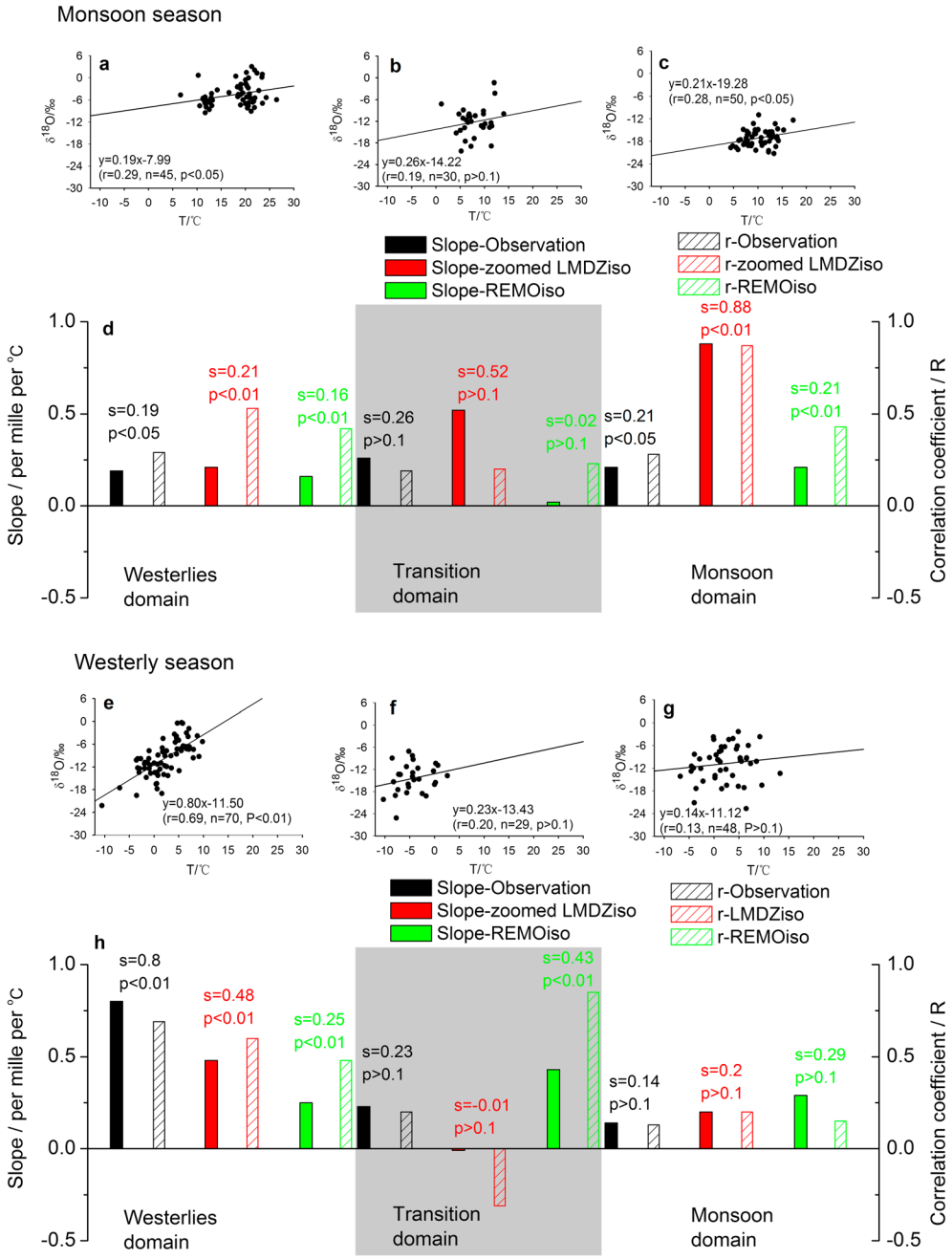

Figure 13. Regressions of observed precipitation $\delta^{18}O$ with temperature based on monsoon (June–September) and westerly (October–May) seasonal data, and corresponding simulated slopes and correlation coefficients at the three domains (the westerlies domain, the transition domain, and the monsoon domain). (a–c) The $\delta^{18}O$-temperature regressions for the three domains based on weighted average data during monsoon season; (d) comparisons between the simulated and observed slopes and correlation coefficients in the three domains. (e–h) Same as Figures 13a–13d but for westerly season. "s" stands for slopes and "p" for the significance level of a Pearson test.

the altitude distribution of precipitation $\delta^{18}O$ appear more ambiguous in the transition domain, possibly because of the sparse data coverage, complex topography, or other factors including shifting seasonal and subseasonal influences of the westerlies and Indian monsoon in this region.

[52] The $\delta^{18}O$ data for Urumqi were excluded from the analysis because of its position (~5° latitudinal difference) and the difficulty to separate elevation and latitude effects. The altitude effect varies seasonally (Figures 15a and 15b). In the westerlies domain, the altitudinal $\delta^{18}O$ lapse rate varies from −0.13‰/100 m during the monsoon season to −0.24‰/100 m during the westerly season. In the monsoon domain, the slope is weak during the westerly season (−0.12‰/100 m) and reaches −0.22‰/100 m during the monsoon season. In the transition domain, similar slopes are depicted (−0.16‰/100 m during monsoon season to −0.20‰/100 m during westerly season). The larger lapse rates in the monsoon domain during monsoon season and the westerlies domain

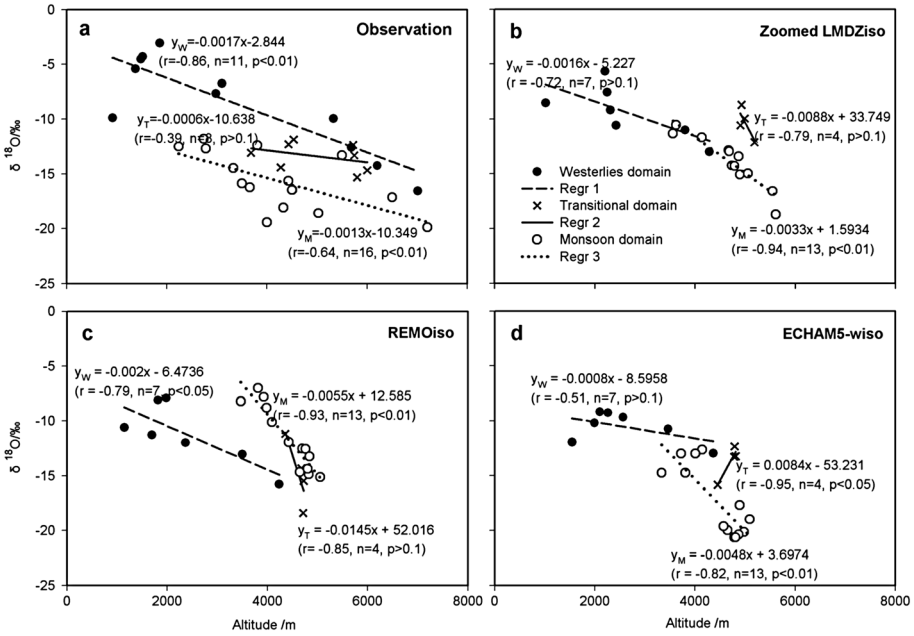

Figure 14. Observed and simulated variations of annual precipitation $\delta^{18}O$ as a function of altitude. The best simulation is done in the westerlies domain. The observed slope of −0.0017‰/m (or −0.17‰/100 m) in the (a) westerlies domain is well simulated (−0.0016‰/m, or −0.16‰/100 m) by the (b) zoomed LMDZiso, roughly simulated (−0.002‰/m, or −0.2‰/100 m) by (c) REMOiso, and poorly simulated (−0.0008‰/m, or −0.08‰/100 m) by (d) ECHAM5-wiso. Results of linear trends are shown as lines and equations. Each data point is an average over the full available period for each station, and for intervals listed in Table 2 for ice cores. Subscripts "W," "T," and "M" are, respectively, for the westerlies domain, the transition domain, and the monsoon domain.

during westerly season are close to the average global lapse rate of −0.28‰/100 m in mid-low latitude mountains [*Poage and Chamberlain*, 2001] and lie within the range of values previously reported in the TP (from −0.12‰/100 m to −0.4‰/100 m) [*Hou et al*., 2003b; *Li et al*., 2006]. The different slopes obtained in different domains and their seasonal variations demonstrate that they are strongly affected by moisture transportation paths.

5.2. Simulations of Altitude Effect

[53] Our three models do capture the observed annual patterns of altitudinal lapse rates over the TP (Figures 14b–14d). Compared with observed lapse rates of −0.17‰/100 m in the westerlies domain, −0.06‰/100 m in the transition domain, and −0.13‰/100 m in the monsoon domain, models perform better in the westerlies domain (−0.16‰/100 m for zoomed LMDZiso, −0.2‰/100 m for REMOiso, and −0.08‰/100 m for ECHAM5-wiso), while there are larger overestimations in other domains, particularly in the transition domain (−0.88‰/100 m for zoomed LMDZiso, −1.45‰/100 m for REMOiso, and −0.84‰/100 m for ECHAM5-wiso) (Figures 14b–14d).

[54] As the sole dominance of either the Indian monsoon (monsoon season) or westerlies (westerly season) displays most obvious temperature effect in different domains as discussed above, similar analysis is done for altitude effect. Six observed lapse rates can be obtained (−0.13‰/100 m for monsoon season and −0.24‰/100 m for westerly season in the westerlies domain, 0.16‰/100 m for monsoon season and −0.20‰/100 m for westerly season in the transition domain, and −0.22‰/100 m for monsoon season and −0.12‰/100 m for westerly season in the monsoon domain) (Figures 15a and 15b). Similar lapse rates to observations are simulated by zoomed LMDZiso (−0.08‰/100 m and −0.18‰/100 m) and REMOiso (−0.14‰/100 m and −0.27‰/100 m) during both the monsoon and westerly seasons in the westerlies domain. In the monsoon domain, zoomed LMDZiso basically simulates observed lapse rates with values of −0.33‰/100 m and −0.10‰/100 m during the monsoon and westerly seasons (Figures 15c and 15d). However, REMOiso always overestimates the lapse rate (−0.48‰/100 m and −0.71‰/100 m) during the monsoon and westerly seasons in the monsoon domain (Figures 15e and 15f). All the models fail to simulate the observed lapse rates in the transition domain.

[55] The above discussions imply that seasonality and atmospheric circulations must be considered for paleo-elevation reconstructions, particularly in the monsoon domain. It also implies that the capabilities of models are crucial to produce reliable simulations. In this study, zoomed LMDZiso shows the best performance on altitude effect, compared with other models.

6. CONCLUSIONS AND PERSPECTIVES

[56] In this review, we have established a comprehensive database of precipitation $\delta^{18}O$ over the TP. Our synthesis explores the influences of the westerlies and Indian monsoon on recent precipitation $\delta^{18}O$ over the TP and identifies three domains with distinct seasonal $\delta^{18}O$ features driven by large-scale atmospheric moisture flux, i.e., the westerlies domain,

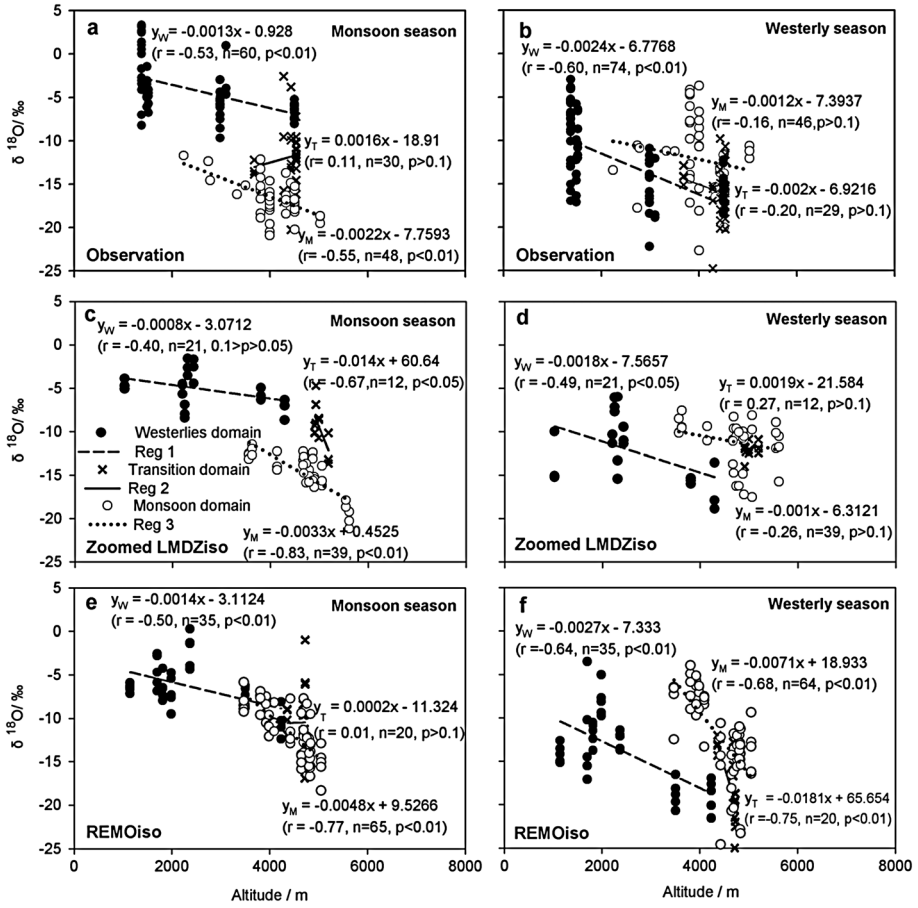

Figure 15. Relationships between observed $\delta^{18}O$ (‰) and altitude (m) in the westerlies domain, the transition domain, and the monsoon domain during (a) monsoon (JJAS) and (b) westerly (October–May) seasons. (c and d) Same as Figures 15a and 15b but for zoomed LMDZiso. (e and f) Same as Figures 15a and 15b but for REMOiso. Notation of the subscripts is the same as in Figure 14.

the transition domain, and the monsoon domain. In the monsoon domain, the shift of the moisture source between BOB and southern Indian Ocean impacts on precipitation $\delta^{18}O$ with the latter resulting in the most depleted $\delta^{18}O$ values. Our database reveals distinct seasonal patterns of temperature and precipitation amount effects in the three different domains. In the westerlies domain, there is a positive relationship between $\delta^{18}O$ and temperature at all time scales. The most significant temperature effect exists when either the westerlies or Indian monsoon is the sole dominant atmospheric process. Different altitude-$\delta^{18}O$ lapse rates in different domains (westerlies domain versus monsoon domain) show large seasonal variations. The wide coverage of precipitation $\delta^{18}O$ from 900 m to above 7000 m asl demonstrates clearly that the lapse rate in the westerlies domain is larger than that in the monsoon domain.

[57] State of the art atmospheric models equipped with the explicit modeling of water isotopes enable to understand the processes and quantify the mechanism that influences the precipitation $\delta^{18}O$ over the TP. All the models capture the impact of the westerlies and monsoon circulations. Zoomed LMDZiso and ECHAM5-wiso basically reproduce the broad spatial patterns of precipitation $\delta^{18}O$ with low $\delta^{18}O$ in the southern TP where the Indian monsoon dominates and with high $\delta^{18}O$ in the northern TP where the westerlies dominate. All the models also reproduce qualitatively the different intraseasonal and seasonal patterns of precipitation $\delta^{18}O$ in the three domains and capture correctly the magnitude of the relationship between precipitation $\delta^{18}O$ and temperature in the westerlies domain. Compared with other two models, zoomed LMDZiso not only shows its better capacity to simulate observation in the TP but also has a potential in demonstrating moisture transport. All the models successfully reproduce the altitude effect in the westerlies domain. However, they have a drier bias in the northern TP, together with a wetter bias in the southern TP, which are common to most climate models [*Su et al*., 2013]. Models overestimate temperature effect in the transition and monsoon domains and fail to correctly simulate relationships between $\delta^{18}O$ and precipitation amount in the monsoon domain. The three models cannot represent quantitatively the lapse rates in the transition and monsoon domains. These biases call for further investigations of the processes at play (convection, subsidence, recycling, and reevaporation) at the event scale. Further studies with longer simulations are needed to assess the local versus large-scale controls of TP precipitation

$\delta^{18}O$ at interannual and longer time scales [*Pausata et al.*, 2011]. A process-based evaluation of the parameterizations of isotopic atmospheric models requires confirmed measurements of precipitation, surface, and vertical profiles of water vapor isotopic composition [*Lee et al.*, 2011; *Risi et al.*, 2010a]. Observations and analyses of vertical profiles of $\delta^{18}O$ in atmospheric vapor may allow to better understand the causes for model-data mismatches.

[58] Our review is of significance for paleoclimate studies as it provides a calibration reference. It aims at motivating a synthesis of paleoclimate information on past $\delta^{18}O$ variability using natural archives and intercomparison of paleoclimate simulations including water stable isotopes, spanning a variety of different climate and topographic boundary conditions.

[59] Our data also provide useful information for hydrology studies. The specific spatial and seasonal patterns identified in precipitation $\delta^{18}O$ in different domains will help to assess the spatial and temporal origin of water resources, using complementary information from glacier meltwater, river, and groundwater $\delta^{18}O$ data.

[60] Many questions remain open regarding the quantitative understanding of the impacts of the westerlies and Indian monsoon circulations on precipitation $\delta^{18}O$ from local to regional scales. It is essential to maintain a long-term monitoring effort, in order to expand the spatial and temporal coverage of precipitation $\delta^{18}O$ databases and achieve a continuous monitoring of air masses along their moisture transport paths, from oceanic source regions toward the TP interior. The model and data mismatch calls for a particular focus on the southern TP and more broadly on the Indian Ocean. A deepened understanding of the physical processes driving the temporal variability of precipitation $\delta^{18}O$ (e.g., convection, subsidence, recycling, reevaporation, and changes in moisture sources) is expected from systematic combination of investigations including $\delta^{18}O$, δD, and $\delta^{17}O$ [*Landais et al.*, 2010]. High-frequency monitoring of water vapor isotopic composition, now available with optical methods even for low-humidity levels [*Galewsky et al.*, 2011; *Johnson et al.*, 2011; *Steen-Larsen et al.*, 2013], has not yet been deployed in the TP and should bring further insights in the understanding of the processes relating to large-scale transport and precipitation isotopic composition variability [*Tremoy et al.*, 2012]. The comparatively poor model performance on annual mean altitude effect in the monsoon domain strongly questions the use of simulated isotopic lapse rates for paleo-elevation reconstructions. The cause for this mismatch may lie in the representation of the vertical moisture transport in the models and therefore call for improved parameterizations of convection. In addition, satellite data can now document the three-dimensional distribution of the water isotopic composition [*Worden et al.*, 2007, *Frankenberg et al.*, 2009] and bring more direct information about large-scale isotopic controls [*Risi et al.*, 2010a, *Lee et al.*, 2012]. Indicators of convective activity (such as outgoing longwave radiation) should be investigated along moisture transport paths to quantify their relationships with precipitation isotopic compositions at event scale and better understand the isotopic controls in the Indian monsoon region [*Risi et al.*, 2008a; *Vimeux et al.*, 2011]. These research directions will improve the documentation, understanding, and simulation of processes controlling the TP precipitation $\delta^{18}O$.

[61] **ACKNOWLEDGMENTS.** This work is supported by CAS Strategic Priority Research Program(B)- Interactions among Multiple Geo-spheres on Tibetan Plateau and their Resource-Environment Effects (grant XDB03000000), the National Natural Science Foundation of China (grants 41190081, 41101061, 40830638, 40971049, and 41371089), the External Cooperation Program of the Chinese Academy of Sciences (grant GJHZ0960), the CAS/SAFEA International Partnership Program for Creative Research Teams, the Cai Yuanpei program, and the GIS Pluies-Tibet. We thank Naoyuki Kurita for his constructive comments. Special thanks are given to anonymous reviewers for very helpful suggestions. Our thanks are also given to all those involved with precipitation sample collections and Tibetan Plateau Scientific Data Sharing Platform.

[62] The Editor, Eelco Rohling, would like to thank two anonymous reviewers for their assistance with this manuscript.

REFERENCES

Aggarwal, P. K., K. Fröhlich, K. M. Kulkarni, and L. L. Gourcy (2004), Stable isotope evidence for moisture sources in the Asian summer monsoon under present and past climate regimes, *Geophys. Res. Lett.*, *31*, L08203, doi:10.1029/2004GL019911.

Aizen, V., E. Aizen, J. Melack, and T. Martma (1996), Isotopic measurements of precipitation on central Asian glaciers (southeastern Tibet, northern Himalayas, central Tien Shan), *J. Geophys. Res.*, *101*(D4), 9185–9196, doi:10.1029/96JD00061.

An, Z., et al. (2012), Interplay between the Westerlies and Asian monsoon recorded in Lake Qinghai sediments since 32 ka, *Sci. Rep.*, *2*, 619, doi:10.1038/srep00619.

An, Z., J. E. Kutzbach, W. L. Prell, and S. C. Porter (2001), Evolution of Asian monsoons and phased uplift of the Himalaya-Tibetan Plateau since Late Miocene times, *Nature*, *411*, 62–66, doi:10.1038/35075035.

Araguás-Araguás, L., K. Froehlich, and K. Rozanski (1998), Stable isotope composition of precipitation over Southeast Asia, *J. Geophys. Res.*, *103*(D22), 28,721–28,742, doi:10.1029/98JD02582.

Barnett, T. P., J. C. Adam, and D. P. Lettenmaier (2005), Potential impacts of a warming climate on water availability in snow-dominated regions, *Nature*, *438*(7066), 303–309, doi:10.1038/nature04141.

Bates, B. C., Z. W. Kundzewicz, S. Wu, and J. P. Palutikof (2008), *Climate Change and Water*, IPCC Secretariat, Geneva, Switzerland.

Bershaw, J., S. M. Penny, and C. N. Garzione (2012), Stable isotopes of modern water across the Himalaya and eastern Tibetan Plateau: Implications for estimates of paleoelevation and paleoclimate, *J. Geophys. Res.*, *117*, D02110, doi:10.1029/2011JD016132.

Bolch, T., A. Kulkarni, A. Kääb, C. Huggel, F. Paul, J. G. Cogley, and M. Scheel (2012), The state and fate of Himalayan glaciers, *Science*, *336*(6079), 310–314, doi:10.1126/science.1215828.

Bothe, O., K. Fraedrich, and X. H. Zhu (2011), Large-scale circulations and Tibetan Plateau summer drought and wetness in a high-resolution climate model, *Int. J. Climatol.*, *31*(6), 832–846, doi:10.1002/joc.2124.

Cai, Y., H. Cheng, Z. An, R. L. Edwards, X. Wang, L. Tan, and J. Wang (2010), Large variations of oxygen isotopes in precipitation over south-central Tibet during Marine Isotope Stage 5, *Geology*, *38*(3), 243–246, doi:10.1130/G30306.1.

Cheruy, F., A. Campoy, J.-C. Dupont, A. Ducharne, F. Hourdin, M. Haeffelin, M. Chiriaco, and A. Idelkadi (2012), Combined influence of atmospheric physics and soil hydrology on the simulated meteorology at the SIRTA atmospheric observatory, *Clim. Dyn.*, doi:10.1007/s00382-012-1469-y.

Craig, H., and L. I. Gordon (1965), Deuterium and oxygen 18 variations in the ocean and the marine atmosphere, in *Stable Isotopes in Oceanographic Studies and Paleotemperatures*, edited by E. Tongiorgi, V. Lischi, Pisa, Italy, pp. 9–130.

Dansgaard, W. (1964), Stable isotopes in precipitation, *Tellus*, *16*(4), 436–468, doi:10.1111/j.2153-3490.1964.tb00181.x.

Frankenberg, C., et al. (2009), Dynamic processes governing lower tropospheric HDO/H_2O ratios as observed from space and ground, *Science*, *325*, 1374–1377, doi:10.1126/science.1173791.

Galewsky, J., C. Rella, Z. Sharp, K. Samuels, and D. Ward (2011), Surface measurements of upper tropospheric water vapor isotopic composition on the Chajnantor Plateau, Chile, *Geophys. Res. Lett.*, *38*, L17803, doi:10.1029/2011GL048557.

Gao, J., L. D. Tian, Y. Q. Liu, and T. L. Gong (2009), Oxygen isotope variation in the water cycle of the Yamzho lake Basin in southern Tibetan Plateau, *Chin. Sci. Bull.*, *54*(16), 2758–2765, doi:10.1007/s11434-009-0487-6.

Gao, J., V. Masson-Delmotte, T. Yao, L. Tian, C. Risi, and G. Hoffmann (2011), Precipitation water stable isotopes in the south Tibetan Plateau: Observations and modeling, *J. Clim.*, *24*, 3161–3178, doi:10.1175/2010JCLI3736.1.

Gardelle, J., E. Berthier, and Y. Arnaud (2012), Slight mass gain of Karakoram glaciers in the early twenty-first century, *Nat. Geosci.*, *5*, 322–325, doi:10.1038/ngeo1450.

Hoffmann, G., M. Werner, and M. Heimann (1998), Water isotope module of the ECHAM atmospheric general circulation model: A study on timescales from days to several years, *J. Geophys. Res.*, *103*(D14), 16,871–16,896, doi:10.1029/98JD00423.

Hou, S., D. Qin, C. P. Wake, P. A. Mayewski, J. Ren, and Q. Yang (2000), Climatological significance of an ice core net-accumulation record at Mt. Qomolangma (Everest), *Chin. Sci. Bull.*, *45*(3), 259–264, doi:10.1007/BF02884687.

Hou, S., D. Qin, T. Yao, D. Zhang, and T. Chen (2002), Recent change of the ice core accumulation rates on the Qinghai-Tibetan Plateau, *Chin. Sci. Bull.*, *47*(20), 1746–1749, doi:10.1007/BF03183321.

Hou, S., D. Qin, D. Zhang, S. Kang, P. A. Mayewski, and C. P. Wake (2003a), A 154a high-resolution ammonium record from the Rongbuk Glacier, north slope of Mt. Qomolangma (Everest), Tibet-Himal region, *Atmos. Environ.*, *37*(5), 721–729, doi:10.1016/S1352-2310(02)00582-4.

Hou, S., V. Masson-Delmotte, D. Qin, and J. Jouzel (2003b), Modern precipitation stable isotope vs. elevation gradients in the High Himalaya. Comment on "A new approach to stable isotope-based paleoaltimetry: Implications for paleoaltimetry and paleohypsometry of the High Himalaya since the Late Miocene" by David B. Rowley et al. [Earth Planet. Sci. Lett. 188 (2001), 253–268], *Earth Planet. Sci. Lett.*, *209*(3–4), 395–399, doi:10.1016/S0012-821X(03)00043-8.

Hren, M. T., B. Bookhagen, P. M. Blisniuk, A. L. Booth, and C. P. Chamberlain (2009), $\delta^{18}O$ and δD of streamwaters across the Himalaya and Tibetan Plateau: Implications for moisture sources and paleoelevation reconstructions, *Earth Planet. Sci. Lett.*, *288*(1–2), 20–32, doi:10.1016/j.epsl.2009.08.041.

Immerzeel, W., L. P. H. van Beek, and M. F. P. Bierkens (2010), Climate change will affect the Asian water towers, *Science*, *328*(5984), 1382–1385, doi:10.1126/science.1183188.

Jacob, T., J. Wahr, W. T. Pfeffer, and S. Swenson (2012), Recent contributions of glaciers and ice caps to sea level rise, *Nature*, *482*(7386), 514–518, doi:10.1038/nature10847.

Johnson, L. R., Z. D. Sharp, J. Galewsky, M. Strong, A. D. Van Pelt, F. Dong, and D. Noone (2011), Hydrogen isotope correction for laser instrument measurement bias at low water vapor concentration using conventional isotope analyses: Application to measurements from Mauna Loa Observatory, Hawaii, *Rapid Commun. Mass Spectrom.*, *25*, 608–616, doi:10.1002/rcm.4894.

Joseph, P. V., K. P. Sooraj, and C. K. Rajan (2006), The summer monsoon onset process over south Asia and an objective method for the date of monsoon onset over Kerala, *Int. J. Climatol.*, *26*, 1871–1893, doi:10.1002/joc.1340.

Joswiak, D. R., T. Yao, G. Wu, B. Xu, and W. Zheng (2010), A 70-yr record of oxygen-18 variability in an ice core from the Tanggula Mountains, central Tibetan Plateau, *Clim. Past*, *6*, 219–227, doi:10.5194/cp-6-219-2010.

Joussaume, S., R. Sadourny, and J. Jouzel (1984), A general circulation model of water isotope cycles in the atmosphere, *Nature*, *311*(5981), 24–29, doi:10.1038/311024a0.

Jouzel, J., G. L. Russell, R. J. Suozzo, R. D. Koster, J. W. C. White, and W. S. Broecker (1987), Simulations of the HDO and $H_2{}^{18}O$ atmospheric cycles using the NASA GISS general circulation model: The seasonal cycle for present-day conditions, *J. Geophys. Res.*, *92*(D12), 14,739–14,760, doi:10.1029/JD092iD12p14739.

Kalnay, E., et al. (1996), The NCEP/NCAR 40-year reanalysis project, *Bull. Am. Meteorol. Soc.*, *77*(3), 437–471, doi:10.1175/1520-0477(1996)077<0437:TNYRP>2.0.CO;2.

Kang, S., Y. Zhang, D. Qin, J. Ren, Q. Zhang, B. Grigholm, and P. A. Mayewski (2007), Recent temperature increase recorded in an ice core in the source region of Yangtze River, *Chin. Sci. Bull.*, *52*(6), 825–831, doi:10.1007/s11434-007-0140-1.

Kang, S., Y. Xu, Q. You, W.-A. Flügel, N. Pepin, and T. Yao (2010), Review of climate and cryospheric change in the Tibetan Plateau, *Environ. Res. Lett.*, *5*, 015101, doi:10.1088/1748-9326/5/1/015101.

Klein, J. A., J. Harte, and X.-Q. Zhao (2004), Experimental warming causes large and rapid species loss, dampened by simulated grazing, on the Tibetan Plateau, *Ecol. Lett.*, *7*(12), 1170–1179, doi:10.1111/j.1461-0248.2004.00677.x.

Klein, S. A., X. Jiang, J. Boyle, S. Malyshev, and S. Xie (2006), Diagnosis of the summertime warm and dry bias over the U.S. Southern Great Plains in the GFDL climate model using a weather forecasting approach, *Geophys. Res. Lett.*, *33*, L18805, doi:10.1029/2006GL027567.

Kurita, N., A. Sugimoto, Y. Fujii, T. Fukazawa, V. Makarov, O. Watanabe, K. Ichiyanagi, A. Numaguti, and N. Yoshida (2005), Isotopic composition and origin of snow over Siberia, *J. Geophys. Res.*, *110*, D13102, doi:10.1029/2004JD005053.

Landais, A., G. Dreyfus, E. Capron, V. Masson-Delmotte, M. F. Sanchez-Goñi, S. Desprat, G. Hoffmann, J. Jouzel, M. Leuenberger, and S. Johnsen (2010), What drives the millennial and orbital variations of $\delta^{18}O_{atm}$?, *Quaternary Sci. Rev.*, *29*(1–2), 235–246, doi:10.1016/j.quascirev.2009.07.005.

Lee, J., J. Worden, D. Noone, K. Bowman, A. Eldering, A. LeGrande, J. L. F. Li, G. Schmidt, and H. Sodemann (2011), Relating tropical ocean clouds to moist processes using water vapor isotope measurements, *Atmos. Chem. Phys.*, *11*(2), 741–752, doi:10.5194/acp-11-741-2011.

Lee, J.-E., C. Risi, I. Fung, J. Worden, R. A. Scheepmaker, B. Lintner, and C. Frankenberg (2012), Asian monsoon hydrometeorology from TES and SCIAMACHY water vapor isotope measurements and LMDZ simulations: Implications for speleothem climate record interpretation, *J. Geophys. Res.*, *117*, D15112, doi:10.1029/2011JD017133.

Lee, J.-E., I. Fung, D. J. DePaolo, and C. C. Henning (2007), Analysis of the global distribution of water isotopes using the NCAR atmospheric general circulation model, *J. Geophys. Res.*, *112*, D16306, doi:10.1029/2006JD007657.

LeGrande, A. N., and G. A. Schmidt (2009), Sources of holocene variability of oxygen isotopes in paleoclimate archives, *Clim. Past*, *5*(3), 441–455, doi:10.5194/cp-5-441-2009.

Li, Z. T., L. Yao, W. Tian, X. G. Yu, and Y. Wang (2006), Variation of $\delta^{18}O$ in precipitation in annual timescale with moisture transport in Delingha region [in Chinese with English abstract], *Earth Sci. Front.*, *13*, 330–334.

Liang, E. Y., X. M. Shao, and Y. Xu (2009), Tree-ring evidence of recent abnormal warming on the southeast Tibetan Plateau, *Theor. Appl. Climatol.*, *98*(1–2), 9–18, doi:10.1007/s00704-008-0085-6.

Liu, X., and B. Chen (2000), Climatic warming in the Tibetan Plateau during recent decades, *Int. J. Climatol.*, *20*, 1729–1742, doi:10.1002/1097-0088(20001130)20:14<1729::AID-JOC556>3.0.CO;2-Y.

Liu, X., J. E. Kutzbach, Z. Liu, Z. An, and L. Li (2003), The Tibetan Plateau as amplifier of orbital-scale variability of the East Asian monsoon, *Geophys. Res. Lett.*, *30*, 1839, doi:10.1029/2003GL017510.

Liu, Z., L. Tian, T. Yao, T. Gong, C. Yin, and W. Yu (2007), Temporal and spatial variations of delta O-18 in precipitation of the Yarlung Zangbo River basin, *J. Geograph. Sci.*, *17*, 317–326, doi:10.1007/s11442-007-0317-1.

Ma, Y., Y. Wang, R. Wu, Z. Hu, K. Yang, M. Li, and H. Ishikawa (2009), Recent advances on the study of atmosphere-land interaction observations on the Tibetan Plateau, *Hydrol. Earth Syst. Sc.*, *13*(7), 1103–1111, doi:10.5194/hess-13-1103-2009.

Masson-Delmotte, V., S. Hou, A. Ekaykin, J. Jouzel, A. Aristarain, et al. (2008), A review of Antarctic surface snow isotopic composition: Observations, atmospheric circulation, and isotopic modeling, *J. Clim.*, *21*(13), 3359–3387.

Mathieu, R., D. Pollard, J. E. Cole, J. W. C. White, R. S. Webb, and S. L. Thompson (2002), Simulation of stable water isotope variations by the GENESIS GCM for modern conditions, *J. Geophys. Res.*, *107*(D4), 4037, doi:10.1029/2001JD900255.

Molnar, P., P. England, and J. Martinod (1993), Mantle dynamics, uplift of the Tibetan Plateau, and the Indian Monsoon, *Rev. Geophys.*, *31*(4), 357–396, doi:10.1029/93RG02030.

Noone, D., and C. Sturm (2010), Comprehensive dynamical models of global and regional water isotope distributions, in *Isoscapes: Understanding Movement, Pattern, and Process on Earth Through Isotope Mapping*, edited by J. B. West, G. J. Bowen, T. E. Dawson, and K. P. Tu, pp. 195–219, Springer, Dordrecht, The Netherlands.

Noone, D., and I. Simmonds (2002), Associations between $\delta^{18}O$ of water and climate parameters in a simulation of atmospheric circulation for 1979–95, *J. Clim.*, *15*, 3150–3169, doi:10.1175/1520-0442(2002)015<3150:ABOOWA>2.0.CO;2.

Pausata, F. S. R., D. S. Battisti, K. H. Nisancioglu, and C. M. Bitz (2011), Chinese stalagmite $\delta^{18}O$ controlled by changes in the Indian monsoon during a simulated Heinrich event, *Nat. Geosci.*, *4*(7), 474–480, doi:10.1038/ngeo1169.

Pfahl, S., H. Wernli, and K. Yoshimura (2012), The isotopic composition of precipitation from a winter storm—A case study with the limited-area model $COSMO_{iso}$, *Atmos. Chem. Phys.*, *12*, 1629–1648, doi:10.5194/acp-12-1629-2012.

Poage, M. A., and C. P. Chamberlain (2001), Empirical relationships between elevation and the stable isotope composition of precipitation and surface waters: Considerations for studies of paleoelevation change, *Am. J. Sci.*, *301*, 1–15, doi:10.2475/ajs.301.1.1.

Poulsen, C. J., and M. L. Jeffery (2011), Climate change imprinting on stable isotopic compositions of high-elevation meteoric water cloaks past surface elevations of major orogens, *Geology*, *39*(6), 595–598, doi:10.1130/G32052.1.

Qin, J., K. Yang, S. L. Liang, and X. F. Guo (2009), The altitudinal dependence of recent rapid warming over the Tibetan Plateau, *Clim. Change*, *97*(1–2), 321–327, doi:10.1007/s10584-009-9733-9.

Ramirez, E., et al. (2003), A new Andean deep ice core from Nevado Illimani (6350 m), Bolivia, *Earth Planet. Sci. Lett.*, *212*(3–4), 337–350, doi:10.1016/S0012-821X(03)00240-1.

Risi, C., et al. (2012a), Process-evaluation of tropospheric humidity simulated by general circulation models using water vapor isotopologues: 1. Comparison between models and observations, *J. Geophys. Res.*, *117*, D05303, doi:10.1029/2011JD016621.

Risi, C., et al. (2012b), Process-evaluation of tropospheric humidity simulated by general circulation models using water vapor isotopic observations: 2. Using isotopic diagnostics to understand the mid and upper tropospheric moist bias in the tropics and subtropics, *J. Geophys. Res.*, *117*, D05304, doi:10.1029/2011JD016623.

Risi, C., S. Bony, and F. Vimeux (2008a), Influence of convective processes on the isotopic composition ($\delta^{18}O$ and δD) of precipitation and water vapor in the tropics: 2. Physical interpretation of the amount effect, *J. Geophys. Res.*, *113*, D19306, doi:10.1029/2008JD009943.

Risi, C., S. Bony, F. Vimeux, and J. Jouzel (2010a), Water-stable isotopes in the LMDZ4 general circulation model: Model evaluation for present-day and past climates and applications to climatic interpretations of tropical isotopic records, *J. Geophys. Res.*, *115*, D12118, doi:10.1029/2009JD013255.

Risi, C., S. Bony, F. Vimeux, C. Frankenberg, D. Noone, and J. Worden (2010b), Understanding the Sahelian water budget through the isotopic composition of water vapor and precipitation, *J. Geophys. Res.*, *115*, D24110, doi:10.1029/2010JD014690.

Risi, C., S. Bony, F. Vimeux, L. Descroix, B. Ibrahim, E. Lebreton, I. Mamadou, and B. Sultan (2008b), What controls the isotopic composition of the African monsoon precipitation? Insights from event-based precipitation collected during the 2006 AMMA field campaign, *Geophys. Res. Lett.*, *35*, L24808, doi:10.1029/2008GL035920.

Rowley, D. B., R. T. Pierrehumbert, and B. S. Currie (2001), A new approach to stable isotope-based paleoaltimetry: Implications for paleoaltimetry and paleohypsometry of the high Himalaya since the Late Miocene, *Earth Planet. Sci. Lett.*, *188*(1–2), 253–268, doi:10.1016/S0012-821x(01)00324-7.

Rozanski, K., L. Araguás-Araguás, and R. Gonfiantini (1992), Relation between long-term trends of oxygen-18 isotope composition of precipitation and climate, *Science*, *258*(5084), 981–985, doi:10.1126/science.258.5084.981.

Schmidt, G. A., G. Hoffmann, D. T. Shindell, and Y. Hu (2005), Modeling atmospheric stable water isotopes and the potential for constraining cloud processes and stratosphere-troposphere water exchange, *J. Geophys. Res.*, *110*, D21314, doi:10.1029/2005JD005790.

Schmidt, G. A., A. N. LeGrande, and G. Hoffmann (2007), Water isotope expressions of intrinsic and forced variability in a coupled ocean–atmosphere model, *J. Geophys. Res.*, *112*, D10103, doi:10.1029/2006JD007781.

Schotterer, U., W. Stichler, and P. Ginot (2004), The influence of post-depositional effects on ice core studies: Examples from the Alps, Andes, and Altai, in *Earth Paleoenvironments: Records Preserved in Mid- and Low-Latitude Glaciers*, edited by L. D. Cecil, J. R. Green, and L. G. Thompson, pp. 39–59, Kluwer Acad, Dordrecht, The Netherlands.

Sjolte, J., G. Hoffmann, S. J. Johnsen, B. M. Vinther, V. Masson-Delmotte, and C. Sturm (2011), Modeling the water isotopes in Greenland precipitation 1959–2001 with the mesoscale model REMO-iso, *J. Geophys. Res.*, *116*, D18105, doi:10.1029/2010JD015287.

Steen-Larsen, H. C., et al. (2013), Continuous monitoring of summer surface water vapour isotopic composition above the Greenland Ice Sheet, *Atmos. Chem. Phys. Discuss.*, *13*, 1399–1433, doi:10.5194/acpd-13-1399-2013.

Stichler, W., U. Schotterer, K. Fröhlich, P. Ginot, C. Kull, H. Gäggeler, and B. Pouyaud (2001), Influence of sublimation on stable isotope records recovered from high-altitude glaciers in the tropical Andes, *J. Geophys. Res.*, *106*(D19), 22,613–22,620, doi:10.1029/2001JD900179.

Sturm, C., F. Vimeux, and G. Krinner (2007a), Intraseasonal variability in South America recorded in stable water isotopes, *J. Geophys. Res.*, *112*, D20118, doi:10.1029/2006JD008298.

Sturm, C., G. Hoffmann, and B. Langmann (2007b), Simulation of the stable water isotopes in precipitation over South America: Comparing regional to global circulation models, *J. Clim.*, *20*(15), 3730–3750, doi:10.1175/JCLI4194.1.

Sturm, K., G. Hoffmann, B. Langmann, and W. Stichler (2005), Simulation of $\delta^{18}O$ in precipitation by the regional circulation model $REMO_{iso}$, *Hydrol. Process.*, *19*(17), 3425–3444, doi:10.1002/hyp.5979.

Su, F., X. Duan, D. Chen, Z. Hao, and L. Cuo (2013), Evaluation of the global climate models in the CMIP5 over the Tibetan Plateau, *J. Clim.*, doi:10.1175/JCLI-D-12-00321.1.

Thompson, L. G. (2000), Ice core evidence for climate change in the tropics: Implications for our future, *Quaternary Sci. Rev.*, *19*(1–5), 19–35, doi:10.1016/S0277-3791(99)00052-9.

Thompson, L. G., E. Mosleythompson, M. E. Davis, J. F. Bolzan, J. Dai, T. Yao, N. Gundestrup, X. Wu, L. Klein, and Z. Xie (1989), Holocene-late Pleistocene climatic ice core records from Qinghai-Tibetan Plateau, *Science*, *246*(4929), 474–477, doi:10.1126/science.246.4929.474.

Thompson, L. G., T. Yao, M. E. Davis, K. A. Henderson, E. Mosley-Thompson, P. N. Lin, J. Beer, H. A. Synal, J. ColeDai, and J. F. Bolzan (1997), Tropical climate instability: The last glacial cycle from a Qinghai-Tibetan ice core, *Science*, *276*(5320), 1821–1825, doi:10.1126/science.276.5320.1821.

Thompson, L. G., T. Yao, E. Mosley-Thompson, M. E. Davis, K. A. Henderson, and P. N. Lin (2000), A high-resolution millennial record of the South Asian monsoon from Himalayan ice cores, *Science*, *289*(5486), 1916–1919, doi:10.1126/science.289.5486.1916.

Tian, L., T. Yao, Z. Yang, and J. Pu (1997), A 4-year's observation of $\delta^{18}O$ in precipitation on the Tibetan Plateau, *J. Glacio and Geocryol*, *19*, 32–36.

Tian, L., T. Yao, W. Sun, M. Stievenard, and J. Jouzel (2001a), Relationship between delta D and delta O-18 in precipitation on north and south of the Tibetan Plateau and moisture recycling, *Sci. China Ser. D*, *44*(9), 789–796, doi:10.1007/Bf02907091.

Tian, L., V. Masson-Delmotte, M. Stievenard, T. Yao, and J. Jouzel (2001b), Tibetan Plateau summer monsoon northward extent revealed by measurements of water stable isotopes, *J. Geophys. Res.*, *106*(D22), 28,081–28,088, doi:10.1029/2001JD900186.

Tian, L., T. Yao, P. F. Schuster, J. W. C. White, K. Ichiyanagi, E. Pendall, J. Pu, and W. Yu (2003), Oxygen-18 concentrations in recent precipitation and ice cores on the Tibetan Plateau, *J. Geophys. Res.*, *108*(D9), 4293, doi:10.1029/2002JD002173.

Tian, L., T. Yao, J. W. C. White, W. Yu, and N. Wang (2005), Westerlies moisture transport to the middle of Himalayas revealed from the high deuterium excess, *Chin. Sci. Bull.*, *50*(10), 1026–1030, doi:10.1360/04wd0030.

Tian, L., T. Yao, Z. Li, K. MacClune, G. Wu, B. Xu, Y. Li, A. Lu, and Y. Shen (2006), Recent rapid warming trend revealed from the isotopic record in Muztagata ice core, eastern Pamirs, *J. Geophys. Res.*, *111*, D13103, doi:10.1029/2005JD006249.

Tian, L., T. Yao, K. MacClune, J. W. C. White, A. Schilla, B. Vaughn, R. Vachon, and K. Ichiyanagi (2007), Stable isotopic variations in west China: A consideration of moisture sources, *J. Geophys. Res.*, *112*, D10112, doi:10.1029/2006JD007718.

Tindall, J. C., P. J. Valdes, and L. C. Sime (2009), Stable water isotopes in HadCM3: Isotopic signature of El Niño–Southern Oscillation and the tropical amount effect, *J. Geophys. Res.*, *114*, D04111, doi:10.1029/2008JD010825.

Tremoy, G., F. Vimeux, S. Mayaki, I. Souley, O. Cattani, C. Risi, G. Favreau, and M. Oi (2012), A 1-year long $d^{18}O$ record of water vapor in Niamey (Niger) reveals insightful atmospheric processes at different timescales, *Geophys. Res. Lett.*, *39*, L08805, doi:10.1029/2012GL051298.

Uppala, S. M., et al. (2005), The ERA-40 re-analysis, *Q. J. Roy. Meteor. Soc.*, *131*(612), 2961–3012, doi:10.1256/qj.04.176.

Vimeux, F., R. Gallaire, S. Bony, G. Hoffmann, and J. Chiang (2005), What are the climate controls on δD in precipitation in the Zongo Valley (Bolivia)? Implications for the Illimani ice core interpretation, *Earth Planet. Sci. Lett.*, *240*(2), 205–220, doi:10.1016/j.epsl.2005.09.031.

Vimeux, F., G. Tremoy, C. Risi, and R. Gallaire (2011), A strong control of the South American SeeSaw on the intra-seasonal variability of the isotopic composition of precipitation in the Bolivian Andes, *Earth Planet. Sci. Lett.*, *307*(1–2), 47–58, doi:10.1016/j.epsl.2011.04.031.

Viviroli, D., H. H. Dürr, B. Messerli, M. Meybeck, and R. Weingartner (2007), Mountains of the world, water towers for humanity: Typology, mapping, and global significance, *Water Resour. Res.*, *43*, W07447, doi:10.1029/2006WR005653.

Vuille, M., M. Werner, R. S. Bradley, and F. Keimig (2005), Stable isotopes in precipitation in the Asian monsoon region, *J. Geophys. Res.*, *110*, D23108, doi:10.1029/2005JD006022.

Wang, B., Q. Ding, and P. V. Joseph (2009), Objective definition of the Indian summer monsoon onset, *J. Clim.*, *22*, 3303–3316, doi:10.1175/2008JCLI2675.1.

Wang, N., T. Yao, J. Pu, Y. Zhang, and W. Sun (2006), Climatic and environmental changes over the last millennium recorded in the Malan ice core from the northern Tibetan Plateau, *Sci. China Ser. D*, *49*(10), 1079–1089, doi:10.1007/s11430-006-1079-9.

Wang, Y., E. Kromhout, C. Zhang, Y. Xu, W. Parker, T. Deng, and Z. Qiu (2008), Stable isotopic variations in modern herbivore tooth enamel, plants and water on the Tibetan Plateau: Implications for paleoclimate and paleoelevation reconstructions, *Palaeogeogr. Palaeocl.*, *260*(3–4), 359–374, doi:10.1016/j.palaeo.2007.11.012.

Werner, M., P. M. Langebroek, T. Carlsen, M. Herold, and G. Lohmann (2011), Stable water isotopes in the ECHAM5 general circulation model: Toward high-resolution isotope modeling on a global scale, *J. Geophys. Res.*, *116*, D15109, doi:10.1029/2011JD015681.

Worden, J., D. Noone, K. Bowman, and T. E. Spect (2007), Importance of rain evaporation and continental convection in the tropical water cycle, *Nature*, *445*, 528–532, doi:10.1038/nature05508.

Wu, T., and Z. Qian (2003), The relation between the Tibetan winter snow and the Asian summer monsoon and rainfall: An observational investigation, *J. Clim.*, *16*(12), 2038–2051, doi:10.1175/1520-0442(2003)016<2038:TRBTTW>2.0.CO;2.

Xu, B., et al. (2009), Black soot and the survival of Tibetan glaciers, *Proc. Natl. Acad. Sci. U. S. A.*, *106*(52), 22,114–22,118, doi:10.1073/pnas.0910444106.

Yang, X., B. Xu, W. Yang, D. Qu, and P.-N. Lin (2009), Study of altitudinal lapse rates of $\delta^{18}O$ in precipitation/ river water with seasons on the southeast Tibetan Plateau, *Chin. Sci. Bull.*, *54*(16), 2742–2750, doi:10.1007/s11434-009-0496-5.

Yang X., T. Yao, W. Yang, W. Yu, and D. Qu (2011), Co-existence of temperature and amount effects on precipitation $\delta^{18}O$ in the Asian monsoon region, *Geophys. Res. Lett.*, *38*, L21809, doi:10.1029/2011GL049353.

Yang, X., T. Yao, W. Yang, B. Xu, Y. He, and D. Qu (2012), Isotopic signal of earlier summer monsoon onset in the Bay of Bengal, *J. Clim.*, *25*, 2509–2516, doi:10.1175/JCLI-D-11-00180.1.

Yao, T., and L. G. Thompson (1992), Trends and features of climatic changes in the past 5000 years recorded by the Dunde ice core, *Ann. Glaciol.*, *16*, 21–24.

Yao, T., Z. Xie, X. Wu, and L. G. Thompson (1991), Climatic change since the Little Ice Age recorded by Dunde Ice Cap, *Sci. China (Ser. B)*, *34*(6), 760–767.

Yao, T., K. Jiao, L. Tian, Z. Li, Y. Li, J. Liu, and E. Thompson (1995), Climatic and environmental records in Guliya Ice Cap, *Sci. China Ser. B*, *38*(2), 228–237.

Yao, T., L. G. Thompson, D. Qin, L. Tian, K. Jiao, Z. Yang, and C. Xie (1996a), Variations in temperature and precipitation in the past 2000 a on the Xizang (Tibet) Plateau–Guliya ice core record, *Sci. China Ser. D*, *39*(4), 425–433.

Yao, T., L. G. Thompson, E. Mosley-Thompson, Y. Zhihong, Z. Xingping, and P.-N. Lin (1996b), Climatological significance of $\delta^{18}O$ in north Tibetan ice cores, *J. Geophys. Res.*, *101*(D23), 29,531–29,537, doi:10.1029/96JD02683.

Yao, T., Y. Shi, and L. G. Thompson (1997), High resolution record of paleoclimate since the Little Ice Age from the Tibetan ice cores, *Quatern. Int.*, *37*, 19–23, doi:10.1016/1040-6182(96)00006-7.

Yao, T. D., V. Masson, J. Jouzel, M. Stievenard, W. Z. Sun, and K. Q. Jiao (1999), Relationships between $\delta^{18}O$ in precipitation

and surface air temperature in the Urumqi River Basin, east Tianshan Mountains, China, *Geophys. Res. Lett.*, *26*(23), 3473–3476, doi:10.1029/1999GL006061.

Yao, T., K. Duan, L. Tian, and W. Sun (2000), Accumulation records from the Dasuopu ice core and variations of Indian summer monsoon precipitation in the past 400 years, *Sci. China Ser. D*, *30*(6), 619–627.

Yao, T. D., Z. X. Li, L. G. Thompson, E. M. Thompson, Y. Q. Wang, L. Tian, N. L. Wang, and K. Q. Duan (2006a), $\delta^{18}O$ records from Tibetan ice cores reveal differences in climatic changes, *Ann. Glaciol.*, *43*(1), 1–7, doi:10.3189/172756406781812131.

Yao, T., X. Guo, L. Thompson, K. Duan, N. Wang, J. Pu, B. Xu, X. Yang, and W. Sun (2006b), $\delta^{18}O$ record and temperature change over the past 100 years in ice cores on the Tibetan Plateau, *Sci. China Ser. D*, *49*(1), 1–9, doi:10.1007/s11430-004-5096-2.

Yao, T., J. Pu, A. Lu, Y. Wang, and W. Yu (2007), Recent glacial retreat and its impact on hydrological processes on the Tibetan Plateau, China, and surrounding regions, *Arct. Antarct. Alp. Res.*, *39*(4), 642–650, doi:10.1657/1523-0430(07–510)[YAO]2.0.CO;2.

Yao, T., K. Duan, B. Xu, N. Wang, X. Guo, and X. Yang (2008), Precipitation record since AD 1600 from ice cores on the central Tibetan Plateau, *Clim. Past*, *4*(3), 175–180, doi:10.5194/cp-4-175-2008.

Yoshimura, K., T. Oki, N. Ohte, and S. Kanae (2003), A quantitative analysis of short-term ^{18}O variability with a Rayleigh-type isotope circulation model, *J. Geophys. Res.*, *108*(D20), 4647, doi:10.1029/2003JD003477.

Yoshimura, K., M. Kanamitsu, D. Noone, and T. Oki (2008), Historical isotope simulation using reanalysis atmospheric data, *J. Geophys. Res.*, *113*, D19108, doi:10.1029/2008JD010074.

Yoshimura, K., M. Kanamitsu, and M. Dettinger (2010), Regional downscaling for stable water isotopes: A case study of an atmospheric river event, *J. Geophys. Res.*, *115*, D18114, doi:10.1029/2010JD014032.

Yu, W., T. Yao, L. Tian, Y. Wang, Z. Li, and W. Sun (2006a), Oxygen-18 isotopes in precipitation on the eastern Tibetan Plateau, *Ann. Glaciol.*, *43*, 263–268, doi:10.3189/172756406781812447.

Yu, W., T. Yao, L. Tian, Z. Li, W. Sun, and Y. Wang (2006b), Relationships between $\delta^{18}O$ in summer precipitation and temperature and moisture trajectories at Muztagata, western China, *Sci. China Ser. D*, *49*(1), 27–35, doi:10.1007/s11430-004-5097-1.

Yu, W., T. Yao, L. Tian, Y. Ma, N. Kurita, K. Ichiyanagi, and W. Sun (2007), Stable isotope variations in precipitation and moisture trajectories on the western Tibetan Plateau, China, *Arct. Antarct. Alp. Res.*, *39*(4), 688–693, doi:10.1657/1523-0430(07–511)[YU]2.0.CO;2.

Yu, W., T. Yao, L. Tian, Y. Ma, K. Ichiyanagi, Y. Wang, and W. Sun (2008), Relationships between $\delta^{18}O$ in precipitation and air temperature and moisture origin on a south–north transect of the Tibetan Plateau, *Atmos. Res.*, *87*(2), 158–169, doi:10.1016/j.atmosres.2007.08.004.

Yu, W., Y. Ma, W. Sun, and Y. Wang (2009), Climatic significance of $\delta^{18}O$ records from precipitation on the western Tibetan Plateau, *Chin. Sci. Bull.*, *54*(16), 2732–2741, doi:10.1007/s11434-009-0495-6.

Zhang, X., Y. Shi, and T. Yao (1995), Variational features of precipitation $\delta^{18}O$ in northeast Tibet Plateau, *Sci. China Ser. B*, *38*(7), 854–864.

Zhao, H., T. Yao, B. Xu, Z. Li, and K. Duan (2008), Ammonium record over the last 96 years from the muztagata glacier in Central Asia, *Chin. Sci. Bull.*, *53*(8), 1255–1261, doi:10.1007/s11434-008-0139-2.